# Discovery and Optimization of a Novel Spiropyrrolidine Inhibitor of β-Secretase (BACE1) through Fragment-Based Drug Design

Ivan V. Efremov,* Felix F. Vajdos,* Kris A. Borzilleri, Steven Capetta, Hou Chen, Peter H. Dorff, Jason K. Dutra, Steven W. Goldstein,[†] Mahmoud Mansour, Alexander McColl, Stephen Noell, Christine E. Oborski, Thomas N. O'Connell, Theresa J. O'Sullivan, Jayvardhan Pandit, Hong Wang, BinQing Wei,[‡] and Jane M. Withka

Pfizer Worldwide Research, Groton Laboratories, Eastern Point Road, Groton, Connecticut 06340, United States

ABSTRACT: The aspartyl protease β-secretase, or BACE, has been demonstrated to be a key factor in the proteolytic formation of Aβ-peptide, a major component of plaques in the brains of Alzheimer's disease (AD) patients, and inhibition of this enzyme has emerged as a major strategy for pharmacologic intervention in AD. An X-ray-based fragment screen of Pfizer's proprietary fragment collection has resulted in the identification of a novel BACE binder featuring spiropyrrolidine framework. Although exhibiting only weak inhibitory activity against the BACE enzyme, the small compound was verified by biophysical and NMR-based methods as a bona fide BACE inhibitor. Subsequent optimization of the lead compound, relying heavily on structure-based drug design and computational prediction of physiochemical properties, resulted in a nearly 1000-fold improvement in potency while maintaining ligand efficiency and properties predictive of good permeability and low P-gp liability.

X-ray fragment screen → SBDD

Asp 228   Asp 32

NMR IC$_{50}$ = 1100 μM   NMR IC$_{50}$ = 1 μM
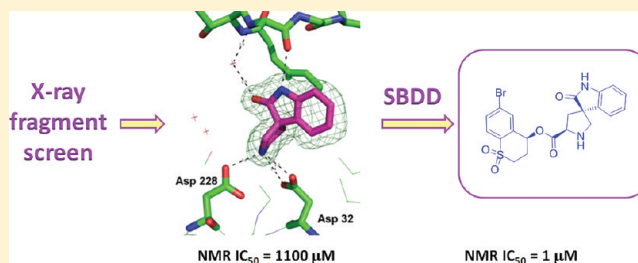
■ INTRODUCTION

Alzheimer's Disease (AD) is a neurodegenerative disorder which is characterized by progressive memory loss and cognitive decline. The hallmarks of this disease are the presence of neurofibrillary tangles along with extracellular amyloid "plaques," composed primarily of proteolytic fragments of amyloid precursor protein (APP).[1] In the early 1990s, researchers reported a genetic link between APP missense mutations and early onset autosomal dominant familial AD.[2] The biological effect of these missense mutations appears to be related to the increased production of the toxic proteolytic fragments leading to plaque formation.[3] In terms of human cost, over 5 million people in the US alone suffer from AD, and nearly 10 million more are expected to develop AD symptoms over the coming decade.[4] The direct cost of providing care for AD patients is more than $148 billion annually, making AD not only a huge human tragedy but an economic problem of enormous magnitude as well.

APP is processed into several short polypeptide fragments through the sequential action of three proteases: α-secretase, β-secretase (BACE), and γ-secretase. BACE (for β-site APP cleaving enzyme) is a type I membrane anchored aspartyl protease within the pepsin family of proteases, while γ-secretase is a complex of at least four membrane-bound proteins:[5] presenilin, nicastrin, Aph1, and Pen2. Sequential processing of APP by BACE and γ-secretase, which liberates a 40−42 residue polypeptide known as Aβ, is mutually exclusive with sequential processing by α-secretase and γ-secretase, which alternatively results in the soluble peptide P3. According to the "amyloid hypothesis," the increased production of Aβ peptides and/or decreased removal of it are the triggers leading to the pathology seen in the brains of AD patients. Hence,

the discovery of inhibitors of this proteolytic cascade has become a major strategic imperative for many pharmaceutical enterprises seeking to develop clinical therapies for this largely unmet medical need.

BACE possesses the now familiar architecture of the pepsin-like aspartyl proteases, one of the smallest protein families in the human genome, with only 15 members.[6] With a bilobal structure, the N- and C-terminal domains of BACE follow a similar topology, consistent with a common evolutionary origin in a gene duplication event.[7] Both domains are highly twisted, eight-stranded β-sheet structures, which are in turn anchored to a six-stranded β-sheet platform. As in all aspartyl proteases, each domain contributes a catalytic aspartic acid residue to the active site machinery, each one directed symmetrically around the protein's pseudo-2-fold axis of symmetry. A catalytic water molecule lies between the two acidic residues, becoming activated by abstraction of a proton in the pH range of 4.5−5.0. This activated water then serves as the nucleophile which cleaves the scissile peptide bond in a substrate polypeptide.[6,8,9] Sequence specificity in the substrate polypeptide is achieved through recognition of side chain residues in the substrate via specificity pockets on the N-terminal side (Sn) and C-terminal side (Sn') of the scissile peptide bond.[10−14]

Screening of low-molecular-weight fragment libraries as a potential source of small, ligand efficient lead matter has

become a standard practice for many drug discovery operations. The utility of fragment screening is especially important for drug targets where the chemical matter of interest has tended to be underrepresented in corporate chemical files such as for aspartyl protease targets. Several groups have published the results of fragment screening campaigns, which have utilized NMR-based methods, bioactivity, biophysical approaches, or X-ray crystallographic screening.[15−19] Although in most of these cases the original lead molecules bound with extremely low potency, often in the low millimolar range, the ligand efficiency was typically quite good owing to their low MW. Structure-based optimization of the original lead compounds has routinely resulted in potencies in the low micromolar range and in some cases even extending into the therapeutically relevant low nanomolar range.[16] While several drug candidates with origin in fragment-based discovery have successfully reached the stage of clinical development, progress in BACE has been slower.[20,21,54] The obvious challenge in fragment-based drug design (FBDD) is to increase potency of hits while simultaneously maintaining properties required for a successful drug candidate. In the context of BACE, the situation is further complicated by the nature of the binding site, which makes development of ligand-efficient inhibitors a significant challenge. From this perspective, selecting the right starting point for lead optimization is paramount.

Many of the early BACE inhibitor classes that have been published in the peer-reviewed literature are peptidomimetics, with transition state isosteres (TSIs) such as hydroxyethylene, statine, hydroxyethylamine (HEA), aminoethylene, and reduced amide. Unfortunately, a majority of these inhibitors tend to possess low ligand efficiency, requiring higher molecular weight in order to gain sufficient potency to inhibit BACE in either in vitro or in vivo assays. The physicochemical properties of these classes of inhibitors therefore tend to exclude them from crossing the blood−brain barrier and make them nearly ideal substrates for efflux pumps such as P-glycoprotein (P-gp).[22] More recently, a number of nonpeptidomimetic scaffolds have been disclosed, including carbinamines,[23] acylguanidines,[24−26] aminoquinazolines,[27] and aminothiazines.[54] While these classes of BACE inhibitors utilize novel interactions with both the catalytic machinery and the specificity pockets of BACE, combining potency, selectivity, brain penetration, and the desired PK profile remains a challenge. Hence, there is a clear need for novel chemical matter to serve as a starting point for development of a potent, selective BACE inhibitor with properties optimal for a CNS drug.[28,29] To address this need, we undertook a fragment screen of our internal collection of small, drug-like fragments[30] using X-ray crystallography as the hit identification platform. These efforts resulted in the discovery of a bona fide BACE inhibitor which possesses an unprecedented spiropyrrolidine core structure, with nearly ideal CNS properties. We also report the optimization of this fragment to achieve potency improvement of 3 orders of magnitude while maintaining the properties consistent with a requirement for good brain penetration.

■ RESULTS AND DISCUSSION

X-Ray Screen. The 340 compounds representing a diverse subset of a proprietary Global Fragment Initiative (GFI) library were soaked as mixtures of four compounds (85 mixtures total). The design of this fragment library has been described in detail.[30] The BACE crystal form utilized was the C222₁ form which has been described previously.[31] This crystal form offers the advantages of a single molecule per asymmetric unit, diffraction to high resolution, and a robust tolerance for various soaking conditions. Initially, the 85 mixtures were tested at 20 mM/compound, with 58 of the resulting soaks yielding useable diffraction data. Subsequently, a second set of experiments was conducted in which the compound concentration was reduced to 2 mM/compound, and later 200 μM/compound, in an attempt to gather data on compound mixtures which appeared to disrupt the crystal lattice at high concentrations. Although diffraction data were obtained for these lower concentration soaks, none resulted in a bound structure. Data were collected at the Sector 17BM beamline at the Advanced Photon Source, Argonne National Lab, Argonne, IL. Data processing was done in an automated fashion using D*trek,[32] followed by refinement using the program AUTOBUSTER.[33]

Identification and the Binding Mode of the Spiro-pyrrolidine Hit 1. Out of the 340 compounds tested, a single compound, the spiropyrrolidine **1**, was clearly visible in the difference density maps (Figure 1). These maps, at a resolution
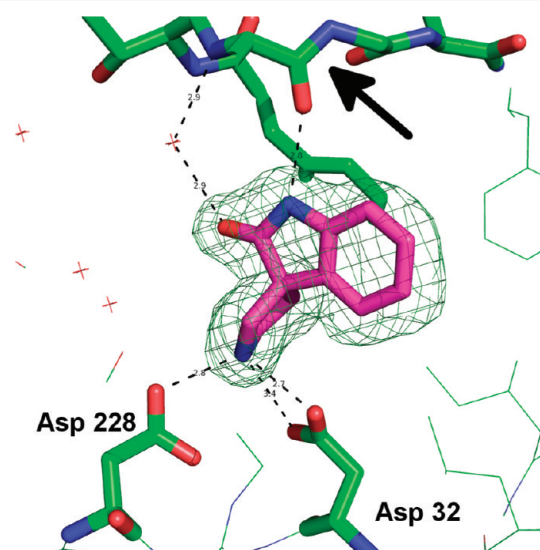
Figure 1. Electron density map ($F_o − F_c$) of **1** bound to BACE. The map is contoured only around **1** at a level of 3σ. The catalytic aspartates Asp32 and Asp228 are indicated as is the Gln73−Gly74 peptide bond (black arrow). Atoms are colored as follows: BACE carbon atoms (green), carbon atoms in **1** (magenta), oxygen (red), nitrogen (blue). Figure generated by Pymol (Schrodinger, LLC).

of 1.71 Å, unambiguously defined the spirocycle of **1**, with the pyrrolidine N sitting squarely between the two catalytic aspartic acids (Asp32 and Asp228 in our structure). Subsequent structures with **1** and derivatives thereof confirmed that the compound identified from this mixture was in fact **1**. The oxindole moiety emanating from the pyrrolidine position 3 sits in the S1 pocket of the BACE active site (Figure 2). This pocket accommodates a wide variety of both aliphatic and aromatic groups. One unusual feature of this binding mode is the fact that the aromatic ring of the oxindole is oriented at an extreme angle relative to the aromatic ring of other BACE inhibitors.[34−36] The aromatic oxindole is approximately parallel to the aromatic side chains of Tyr71 and Phe108 but is displaced from these two ring systems, thus eliminating any aromatic $\pi−\pi$ interactions. The entire inhibitor is well-sequestered within the S1 pocket and offers no vectors to build off of the oxindole to access the adjacent S3 pocket.
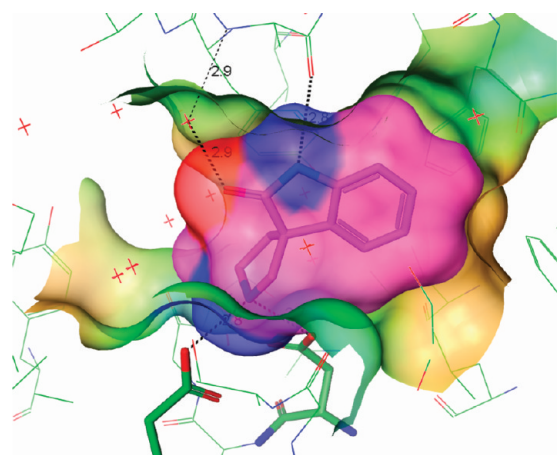
Figure 2. The spiropyrrolidine **1** efficiently fills the S1 pocket of BACE, with extensive hydrogen bonding interactions between the catalytic aspartic acids and flap residues. The protein surface is colored as a spectrum according to hydrophobicity (brown, hydrophobic; blue, polar). The van der Waals surface of **1** is colored as in Figure 1.

A second noteworthy feature of the BACE:**1** complex is the orientation of the peptide bond between flap residues Gln73 and Gly74, which is clearly flipped relative to that seen in many other BACE-inhibitor structures (Figure 1). In the BACE:**1** structure, the carbonyl O atom of Gln73 accepts a hydrogen bond from the oxindole NH of the bound compound, with an interatomic distance of 2.8 Å between the O and N atoms. A similar orientation of this peptide bond is seen in the structure of BACE bound to a carbinamine inhibitor in which the carbonyl O atom accepts a hydrogen bond from the alkyl amine side chain of the bound inhibitor (1TQF).[23] A third example of this orientation for the Gln73−Gly74 peptide bond is seen in the structure of BACE bound to a hydroxyethylene peptidomimetic inhibitor (1FKN), although in that structure the carbonyl does not form a productive hydrogen bond with the bound ligand.

A third feature of the BACE:**1** complex is the orientation of the carboxylate side chain of the catalytic residue Asp32. While in most BACE structures this residue is approximately coplanar with its symmetrical partner Asp228, in this structure the carboxylate is rotated by ∼90° due to a steric clash with the pyrrolidine side chain (Figure 2). This orientation has been observed only rarely in BACE, most notably for the first structure reported for this enzyme, 1FKN, in which the carboxylate group Asp32 is ∼50° out of plane with that of Asp228.[11] The carboxylate group rotates in order to alleviate a potential steric clash with the pyrrolidine ring and may offer a better hydrogen bonding geometry with the lone pair orbitals of the side chain oxygens in this configuration.

Confirmation of 1 as a Bona Fide BACE Inhibitor. Although the crystal structure of **1** clearly indicated a productive binding mode to the catalytic machinery of BACE, it still remained to be established that **1** represented a bona fide inhibitor class in which binding affinity and functional activity could be correlated with structure. As part of our fragment-based drug discovery strategy, multiple biophysical binding and activity assays were developed to reliably assay ligands at high concentrations. The very high compound concentration required for visualization in electron density maps (20 mM) indicated a very weak binding affinity, and this was rapidly confirmed by a competitive biolayer interferrometry experiment,

termed the Octet assay. In this assay, a biotinylated form of a previously described stat-val peptide,[53] which inhibits BACE in the nM range, was synthesized in-house, and captured onto streptavidin-coated sensor tips. This peptide bound to BACE with a K_D = 15 nM, as determined by the Octet assay. Samples of BACE containing a series of concentrations of compound, and a sample of BACE containing no compound, were then allowed to bind to the stat-val peptide. The BACE binding signal produced from the BACE:stat-val interaction was monitored, and a loss of signal as a function of compound concentration was observed for compounds that were bound to the active site of BACE. The K_D of **1** estimated by this method was 1.4 mM, which yields a ligand efficiency (LE) of 0.31 kcal/mol/atom, according to the formula given in Hopkins et al.[37] Consistent with the Octet results, **1** was confirmed to bind reversibly and competitively with a known potent HEA inhibitor of BACE (N-[(1S,2R)-1-[(3,5-difluorophenyl)-methyl]-3-[[4-[3-(1,1-dimethylethyl)phenyl]tetrahydro-2H-pyran-4-yl]amino]-2-hydroxypropyl]-acetamide[42]) using NMR saturation transfer difference (STD) methods.[38] A detailed understanding of the BACE binding site residues involved in interactions with **1** in solution was investigated using [15]N−^{1}H 2D NMR TROSY correlation methods. Published chemical shifts[39] for BACE were mapped to in-house spectra, and site-specific chemical shift perturbations upon ligand binding were identified. Significant perturbation of active site residues including the critical aspartates, Asp32 and Asp228, were observed and were consistent with the X-ray structure. In addition to the binding studies, a functional NMR activity assay for BACE, using a modified peptide substrate NH-SEVNLAAEF-COOH with a reduced K_m = 212 μM (data not published), was developed to generate IC$_{50}$ values for weakly active compounds requiring high ligand concentrations.[44] NMR functional assays have proven useful for atomic level detection of reactants and products with miminal detection artifacts. An added advantage to these methods is the evaluation of the structural and chemical integrity of the ligand. Consistent with binding information, **1** also clearly inhibited BACE enzymatic activity in the NMR-based functional assay with an IC$_{50}$ value of 1.1 mM, thus demonstrating that the scaffold was functionally capable.

Spiropyrrolidine 1 as a Starting Point for Hit to Lead Efforts. Having established the binding profile and functional competency of the spiropyrrolidine **1** as a novel motif for BACE inhibition, we needed to ascertain the validity of this structural class from a lead development perspective. We had particular concerns in regard to the brain penetration potential of the spiropyrrolidine class based on our earlier work on the nonspirocyclic version of pyrrolidine-containing BACE inhibitors.[40] It was found that **1** had excellent permeability profile (MDCK AB = 12.2 × 10^{-6} cm/s) coupled with low potential for P-gp efflux as evidenced by low BA/AB ratio of 0.994 in MDR1-transfected MDCK line. This compared favorably to nonspirocyclic pyrrolidines with similar substitution pattern and molecular weight (data not shown). Ligand efficiency is a key parameter to consider in a lead development process.[41] Compound **1** has a ligand efficiency value of 0.3 kcal/mol/atom, which we considered to be a promising range in light of the nature of the BACE active site. This value contrasted favorably with ligand efficiency of peptidomimetic inhibitors and was in line with more promising BACE binders being disclosed in the literature at the time.[16,17,19,46] To further solidify our confidence in choosing **1** as a starting point for lead optimization efforts, we undertook the following thought

experiment: we have enumerated prospective analogues following the most plausible expansion vectors (vide infra) assuming that we would be able to keep the ligand efficiency value of the hit compound **1**. With this assumption, a significant fraction of potential future targets was predicted to achieve 1 μM potency level while maintaining potential for good brain penetration as assessed by proprietary in silico ADME models. Taken together, these data indicated that the hit **1** represented a valuable opportunity in our search for next generation BACE inhibitors.

Fragment Hit Optimization: Identification of a Growth Vector. The hit assessment process provided a solid confirmation of binding of **1** to BACE and underscored the favorable characteristics of this scaffold for further elaboration into more potent analogues compatible with requirements for brain penetration. The next stage was to define the hit optimization strategy. We envisioned two activities: further optimization of the core (with a goal of increasing ligand efficiency) and identification of growth vectors. The former could prove useful to further enhance binding affinity or drug-like nature of the scaffold while the latter was an absolute requirement for hit-to-lead work. While both avenues were pursued at the same time, the priority clearly was to find a suitable growth direction which effort is described in this manuscript.

As noted above, the phenyl ring of the hit compound occupies the S1 subsite of BACE with high degree of complementarity. At the same time, the position and orientation of the P1 substituent is such that it does not allow a convenient access to the neighboring S3 subsite. We found it to be unfortunate because a majority of more ligand efficient BACE binders feature occupancy of both of these pockets.[16,17,19,41] The other more druggable subsites of the target which could potentially be accessed from this scaffold were S2 and S1′/S2′. The S2 pocket could potentially be accessed from the β-face of position 2 of the pyrrolidine ring. After careful consideration, we concluded that it was a less advantageous option because it would require too many linker atoms to take advantage of the hallmark polar interactions in this subsite. The vector into the prime side of the protein was determined to be more promising based on trajectory offered by the β-face of the pyrrolidine position 5. It was noted that this vector aligned well with HEA type of BACE inhibitors which can achieve promising levels of ligand efficiency by primarily utilizing the prime-side interactions.[42,43] To reach the S1′/S2′ pockets, we considered both flexible and rigid linkers. The former had an advantage of being more forgiving in adopting the required binding conformation while the latter could prove to be more ligand efficient by minimizing entropic penalty from restricting the ligand's degrees of freedom upon binding.

Our initial attempt was to install a flexible linker with a basic amine at the β-position to mimic the trajectory and functionality placement of the HEA inhibitors. Molecular modeling suggested that compound **2a** would be a good test case of this hypothesis while also including a Ph ring to occupy the S2′ pocket. In contrast to our expectations, this compound exhibited no activity in the functional NMR assay at 1 mM concentration. We reasoned that the side chain amine might be protonated first, thus causing basicity change of the key pyrrolidine nitrogen. To address this, compound **2b** was prepared where the pyrrolidine amine is clearly the more basic one and the CF₃ group should be accommodated by the S3′ pocket. This compound was only weakly active, exhibiting 31%

inhibition at 1 mM in the functional NMR assay, which we thought was a minor gain considering the number of heavy atoms added to the scaffold. In addition, the MDR data suggested that further growth of the analogue **2b** would bring P-gp liability. In light of these results, it was decided to explore novel linkers to access the prime side pockets. Expediently, we identified that an array of primary and secondary amides **3a−d** did not produce an evidence of improved binding. The analogues tested included both minimally substituted N-Me derivatives to probe the growth direction and more elaborate ones featuring P1′ and P2′ substituents. Phenyl and amide analogues demonstrated measurable binding. An important conclusion was that it should be possible to expand the fragment **1** along this growth vector while maintaining potential for good brain penetration on the basis of good permeability and low efflux liability (Table 1).

A significant observation was that a simple methyl ester **5** demonstrated a significant level of enzyme inhibition with only minor deterioration in ligand efficiency, NMR IC₅₀ = 242 μM (LE = 0.28 kcal/mol/atom). This finding was especially significant in light of the fact that an X-ray structure of this analogue revealed that it had not yet reached any new Schechter subsites (Figure 3).[10,12,13]

Although the presence of an ester functional group would likely be undesirable in a drug candidate, we reasoned that it could prove useful in exploring the SAR in the prime-side pockets. The above-mentioned Ph analogue **4** demonstrated that an isosteric replacement of the ester group was, in principle, possible.

SAR Exploration of the S1′ and S2′ Subsites. Initial SAR plans in the ester arena were formulated based on the preferred S1′ and S2′ substitution known in the HEA literature. It was reasoned that cyclic nonaromatic substituents had the best chance of productively occupying the S1′ subsite while aromatic substituents were historically preferred for S2′. One of the first analogues targeting occupancy of the S1′ pocket was a tetrahydropyran (THP) derivative **6**. An X-ray crystal structure of **6** revealed that, indeed, the THP moiety was directed toward the S1′ pocket; intriguingly, this was accompanied by a flip of the ester moiety relative to **5** (Figure 4).

It was noted that this compound showed significant improvement in potency without any significant loss of ligand efficiency (Table 2). It is also important to highlight the fact that at this level of enzyme affinity a robust response in a primary biochemical assay, ELISA-based cell-free assay, was detected. The increase in the molecular weight did not cause any deterioration of the in vitro indicators of brain penetration. Quick SAR exploration indicated that further potency increase was possible by modification of the P1′ substituent such as in compound **7** although at the expense of ligand efficiency. Having probed the S1′ subsite, we shifted our attention to the S2′ area of the active site. Again, the key question was whether potency improvement could be achieved without sacrifice in ligand efficiency and ADME profiles. The SAR exploration benefitted from the fact that the same ester function could be used to answer these questions. A simple benzyl ester analogue **8** demonstrated significant potency levels in both NMR and biochemical assays coupled to excellent permeability and MDR efflux parameters. The X-ray crystal structure of **8** indicated that, indeed, the benzyl ester was directed toward the S2′ pocket (Figure 5). The subsequent SAR work has centered on optimization of the P2′ aromatic ring with an objective of increasing ligand efficiency profile of these binders.

Table 1. Initial Results for Hit Expansion Analogues

Compound	R	% inhibition at 1 mM in NMR functional assay	RRCK AB (x10⁻⁶ cm/s)[a]	MDR BA/AB[b]	HLM CL$_{int}$ (μL/min/mg)[c]
2a		8	13.5	1.99	76.7
2b		31	ND[d]	2.51	94.8
3a		20	4.86	ND	14.3
3b		12	ND	1.01	<8.00
3c		27	ND	ND	ND
3d		3	2.92	4.76	<8.00
3e		22	ND	1.87	15.0
4[e]		31	29.6	0.983	16.6

[a]MS-based quantification of the basal/apical transfer rate of a test compound at 2 μM across contiguous monolayers from RRCK cells. [b]Ratio from the MS-based quantification of apical/basal and basal/apical transfer rates of a test compound at 2 μM across contiguous monolayers from MDR1-transfected MDCK cells. [c]Intrinsic clearance from human liver microsomal stability assay. [d]ND: not determined. [e]Tested as a racemic mixture of diastereomers in 6:1 ratio at the position 5 of the pyrrolidine ring.
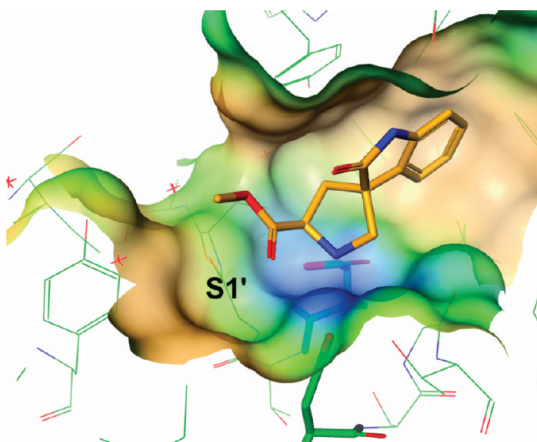
Figure 3. X-ray crystal structure of **5** bound to BACE, with the methyl ester emanating from the pyrrolidine 5 position toward the prime side of the active site.
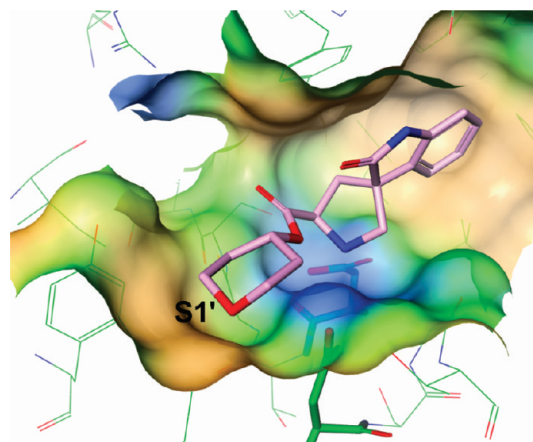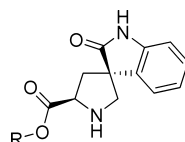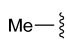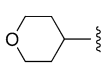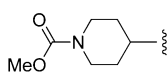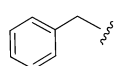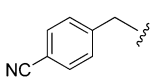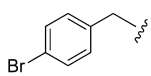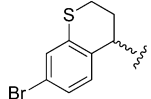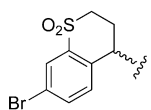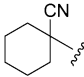

Figure 4. X-ray crystal structure of **6** bound to BACE, with the THP moiety extending toward the S1′ pocket. Note the flip of the ester linker.

It is worth highlighting again that both pockets were explored using the same chemistry. In fact, this could have complicated interpretation of empirical SAR had it not been possible to

routinely obtain X-ray structures for key compounds. Figure 6 demonstrates the binding mode of the benzyl and THP esters (**8** and **6**, correspondingly). It is instructive to observe the

Table 2. Ester SAR

Compound	R	biochemical CFA assay IC$_{50}$ (μM)[a]	NMR functional assay IC$_{50}$ (μM)[b]	NMR LE (kcal/mol/atom)	RRCK AB (x10^{-6} cm/s)[c]	MDR BA/AB
5	Me—	ND[e]	242	0.30	29.5	1.13
6	(tetrahydropyran-4-yl)	114	32	0.28	25	1.02
7	(1-methoxycarbonylpiperidin-4-yl)	83.7	14	0.26	20.9	1.91
8	(benzyl)	85.7	33	0.27	30.4	0.986
9	(4-cyanobenzyl)	12.2[f]	7.0	0.28	18.4	0.913
10	(4-bromobenzyl)	29.5	ND	ND	7.11	2.24
11	(3-bromo-4-cyanobenzyl)	6.26	2.0	0.30	10.2	ND
12	(6-bromothiochroman-4-yl)	22.6	6.0	0.27	ND	ND
13	(6-bromothiochroman-4-yl 1,1-dioxide)	4.00	1.0	0.28	49.1	6.85
14	(1-cyanocyclohexyl)	25.4	11	0.29	22.7	ND

[a]Control compound showed a geometric mean IC$_{50}$ of 58 nM (n = 148) with a 95% confidence interval between 53 and 63 nM. [b]Control compound showed a geometric mean IC$_{50}$ of 30 μM (n = 21) with a 95% confidence interval between 28 and 32 μM. [c]MS-based quantification of the basal/apical transfer rate of a test compound at 2 μM across contiguous monolayers from RRCK cells. [d]Ratio from the MS-based quantification of apical/basal and basal/apical transfer rates of a test compound at 2 μM across contiguous monolayers from MDR1-transfected MDCK cells. [e]ND: not determined. [f]Tested in duplicate.

reversal of the orientation for the ester group and proximity of the ester oxygen atoms to the protonated pyrrolidine nitrogen. An obvious conclusion was to invoke a potential for intramolecular hydrogen bond between these functionalities. Such an observation would be particularly important in future efforts to find ester isosteres.

This structural information has allowed rational design of the next generation of analogues. Derivatives **9** and **10** with cyano and bromo *para*-substituents on the benzyl ring demonstrated improvement in potency, presumably due to interaction with charged guanidinium group of Arg128 (Figure 6). Addition of a *meta*-bromo substituent to better fill the S2′ pocket (Figure 7) led to single-digit micromolar potency in both NMR and biochemical assays (compound **11**).

Derivative **12** was also reasonably potent, but the exact orientation of the ester substituent in the BACE active site was not known: the saturated ring could occupy the S1′ subsite or, alternatively, the aromatic ring could be accommodated by the S2′ pocket. An attempt to obtain an X-ray pose of the bound conformation was successful and confirmed that this compound was bound similar to the other benzylic esters with the P2′ aromatic substituents (Figure 8). Further analysis offered an intriguing possibility of installing interactions with the residues in the flap region (residues 71−75). Indeed, this potential was realized in the derivative **13** which, despite significant increase in polarity, was also noticeably more potent, thus indicating a productive polar interaction, presumably a hydrogen bond between sulfone oxygen and backbone NH of Thr72. We were
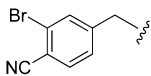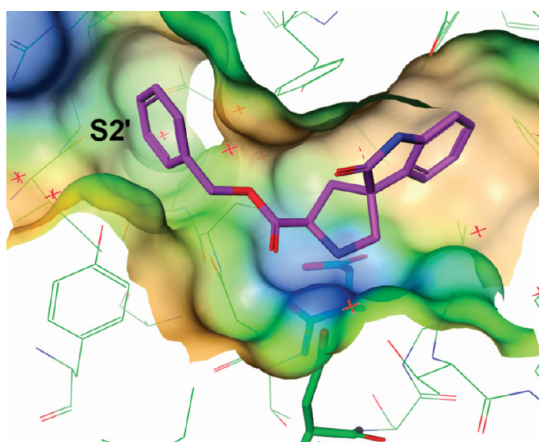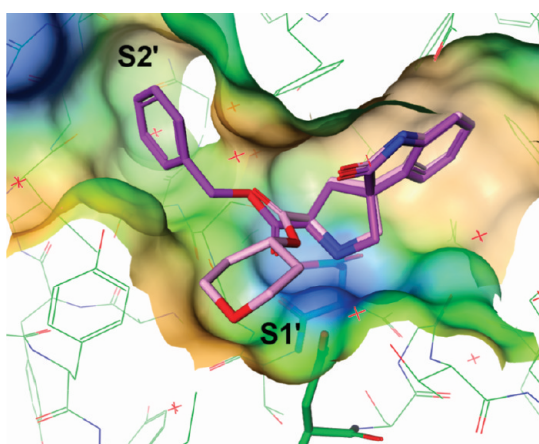
Figure 5. X-ray crystal structure of **8** bound to BACE. The benzyl ester is now oriented toward the S2′ pocket, marked by a corresponding flip in the ester linker to that seen with **5**.


Figure 6. Overlay of X-ray crystal structures of compounds **6** and **8**, illustrating the different trajectories assumed by the THP- and benzyl-esters toward the S1′ and S2′ specificity pockets, respectively.
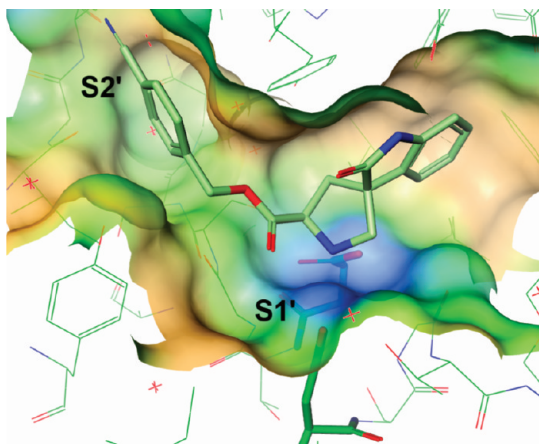
Figure 7. **9** bound to the BACE active site. The 4-cyano benzyl ester is directed toward the S2′ pocket as seen in **8**, with the cyano group making positive electrostatic interactions with the guanidinium group of Arg128.

later successful in obtaining an X-ray structure of a pure diastereomer **13a**, which has clearly shown the successful engineering of a productive hydrogen bond with the flap.

To further expand on this observation, the attention was focused again on the S1′ binders. Synthesis of the cyano
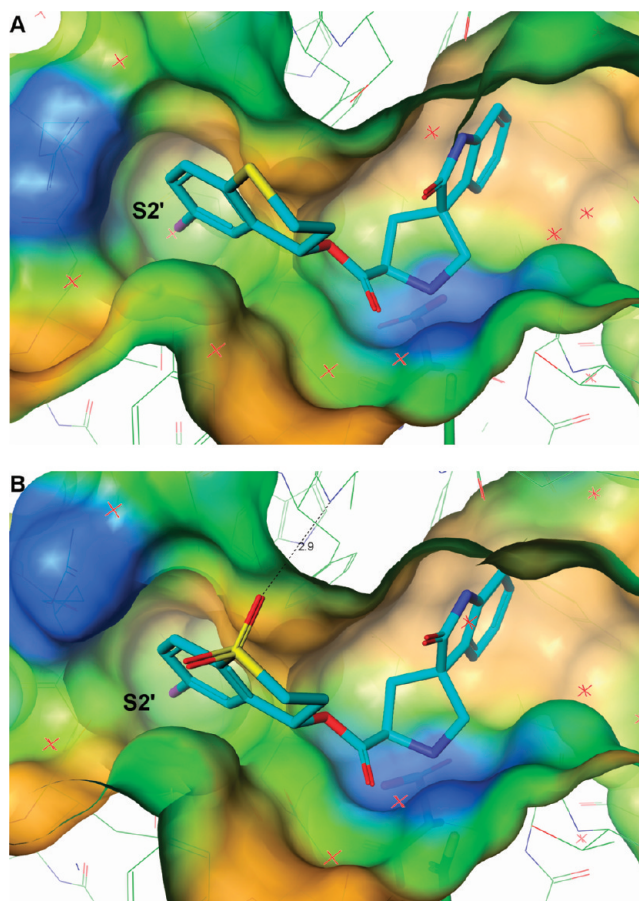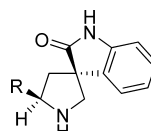
Figure 8. (A) X-ray structure of **12** bound to BACE. The 4-Br thiochromene ester is directed toward the S2′ pocket as in **11**, with the S atom oriented upward toward the flap. (B) Design of **13a** led to productive hydrogen bonding interactions with backbone NH of Thr72.
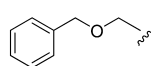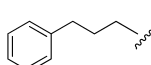
derivative **14** produced a profile similar to **13**, where potency improvement was observed along with the polarity increase. X-ray data for this binder confirmed a presence of a productive hydrogen bond between the CN acceptor and backbone NH of Thr72 as the donor (Figure 9).
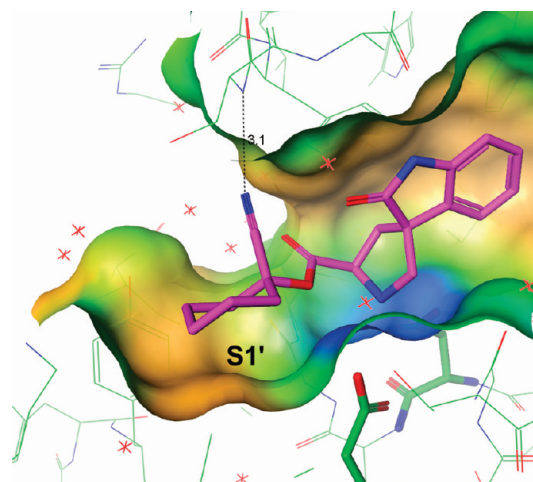
Figure 9. X-ray structure of **14** bound to BACE. The 1-cyano group extends up toward the flap, making similar hydrogen bonds as modeled for the sulfone of **13**.

Table 3. Assessment of Linkers without a Carbonyl Group

Compound	R	% inhibition in NMR functional assay	RRCK AB (x10⁻⁶ cm/s)[a]	MDR BA/AB[b]	hMicCL (ml/min/kg)[c]
15	(benzyl-O-CH2CH2)	23% at 0.2 mM	23.9	1.12	24.7
16	(phenyl-CH2CH2CH2)	41% at 1 mM	11.4	1.25	91.3

[a]MS-based quantification of the basal/apical transfer rate of a test compound at 2 μM across contiguous monolayers from RRCK cells. [b]Ratio from the MS-based quantification of apical/basal and basal/apical transfer rates of a test compound at 2 μM across contiguous monolayers from MDR1-transfected MDCK cells. [c]Predicted hepatic clearance (CLh) from human liver microsomal stability assay.

Scheme 1. Synthesis of (3S,5′R)-1′-(*tert*-Butoxycarbonyl)-2-oxospiro[indoline-3,3′-pyrrolidine]-5′-carboxylic Acid 19 and Esters 5−14[a]

6: R=tetrahydro-2H-pyran-4-yl
7: R=1-(methoxycarbonyl)piperidin-4-yl
8: R=benzyl
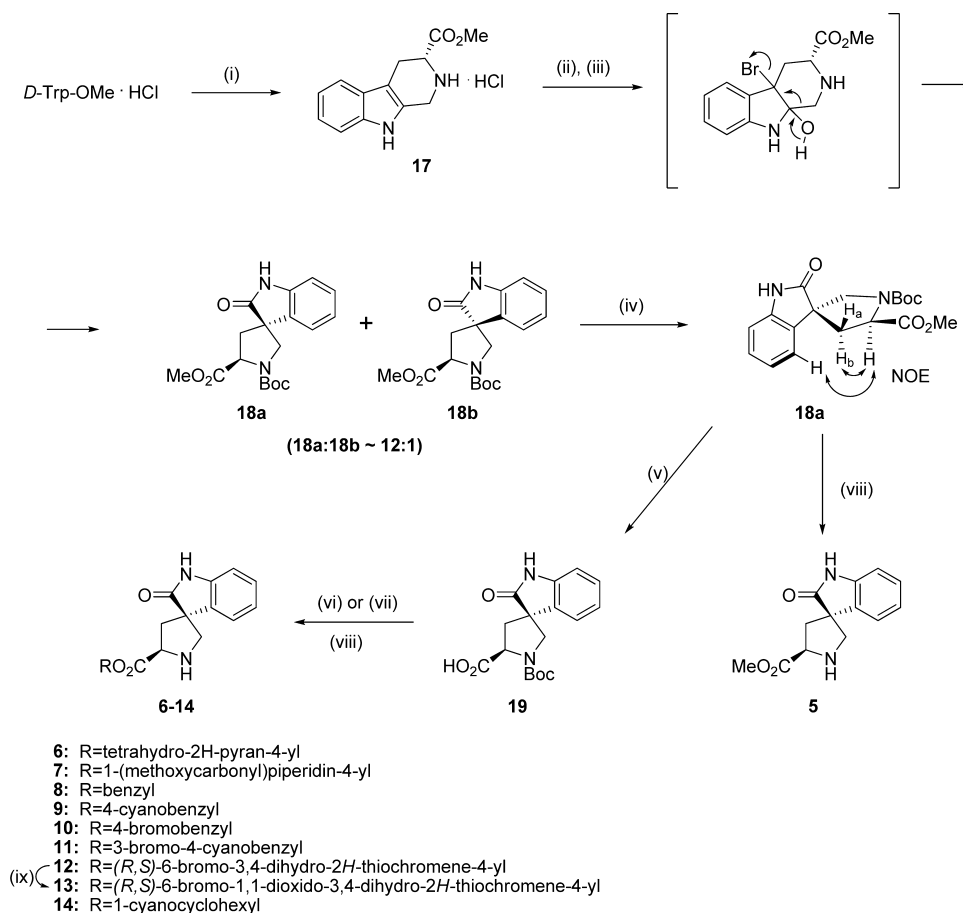9: R=4-cyanobenzyl
10: R=4-bromobenzyl
11: R=3-bromo-4-cyanobenzyl
12: R=(*R,S*)-6-bromo-3,4-dihydro-2*H*-thiochromene-4-yl
13: R=(*R,S*)-6-bromo-1,1-dioxido-3,4-dihydro-2*H*-thiochromene-4-yl
14: R=1-cyanocyclohexyl

(ix) {12, 13}

[a]Reagents and conditions: (i) HCHO/MeOH; (ii) Boc₂O/TEA; (iii) NBS/AcOH; (iv) normal-phase chromatography; (v) LiOH/THF/H₂O; (vi) ROH/DCC/DMAP; (vii) ROH/2,4,6-trichlorobenzoyl chloride/TEA/DMAP; (viii) HCl/dioxane/MeOH; (ix) *m*CPBA/DCM

An initial assessment of the linker types (vide supra) was continued with preparation of derivatives **15** and **16** lacking the ester carbonyl (Table 3). A significant deterioration of potency was observed, further highlighting the importance of having a hydrogen bond acceptor in proximity to the protonated pyrrolidine nitrogen, presumably due the earlier proposal of the intramolecular hydrogen bond.

Importantly, some of the most potent analogues maintained excellent permeability and low predicted P-gp efflux of the starting hit **1**, which was the objective established at the outset of the fragment hit optimization efforts. Also of significance, the potency improved close to 3 orders of magnitude without any significant deterioration of the ligand efficiency profile. These observations bode well for additional

Scheme 2. Synthesis of Sulfone Derivative 13a and 13b[a]
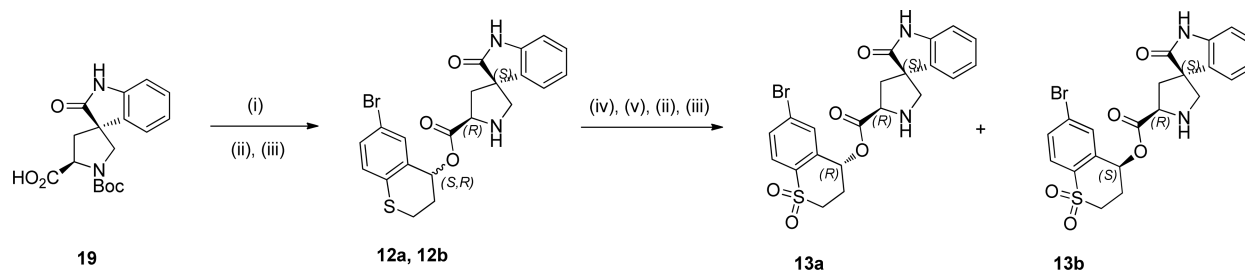
[a]Reagents and conditions: (i) (R,S)-6-bromo-thiochroman-4-ol/DCC/DMAP; (ii) HCl/dioxane/MeOH; (iii) separation; (iv) (Boc)₂O, TEA, THF; (v) mCPBA/DCM.

Scheme 3. Synthesis of [(Benzyl)aminomethyl]spiro[indole-3,3′-pyrrolidin]-2(1H)-ones 2a and 2b[a]
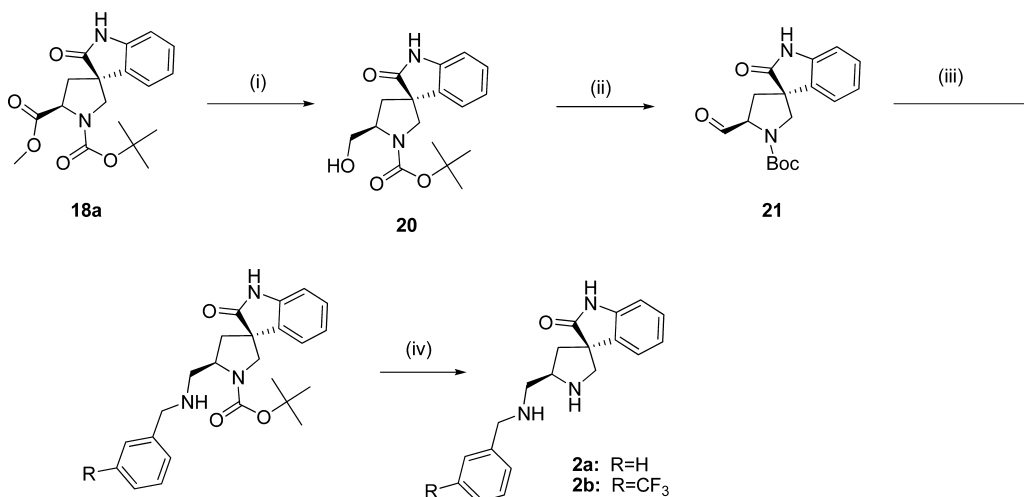
[a]Reagents and conditions: (i) LiBH₄/THF, rt; (ii) Dess−Martin periodinane/DCM; (iii) RC₆H₄CH₂NH₂/NaBH(OAc)₃; (iv) 4 M HCl/dioxane.

optimization work in this series on route to viable BACE inhibitors.

CHEMISTRY

The key transformation for synthesis of the oxindole-containing spirocyclic pyrrolidines was a combination of Pictet−Spengler reaction with oxidative rearrangement of the resulting tetrahydro-β-carboline intermediate.[31−33] Thus, treatment of D-tryptamine methyl ester with formaldehyde in methanol led to the formation of the tetrahydro-β-carboline **17** (Scheme 1). Boc-protection of the amine followed by NBS-induced oxidative rearrangement furnished the desired spirocyclic pyrrolidine intermediate as a mixture of diastereomers. The desired intermediate **18a** could be obtained in pure form by using normal-phase chromatography, and its relative stereochemistry was confirmed by analysis of NOE signals. Removal of the Boc group under acidic conditions led to **5**. Saponification of **18a** followed by ester formation using either DCC or 2,4,6-trichlorobenzoyl chloride as the activating agents followed by Boc deprotection provided analogues **6−12** and **14**. Sulfone analogue **13** was obtained by mCPBA oxidation of the thiochromane derivative **12**.

Individual diastereomers **13a,b** were prepared via a slightly modified sequence of steps. The ester coupling was achieved by application of DCC. Deprotection step was necessary at this stage to obtain individual diastereomers **12a,b** in a pure form which was accomplished by preparative HPLC. Protecting group manipulations in combination with mCPBA oxidation

independently afforded sulfone derivatives **13a** and **13b** (Scheme 2).

Synthesis of amine analogues **2a** and **2b** was accomplished by two-step formation of aldehyde **21** from the key intermediate **18a**. Reductive amination followed by the deprotection step produced the requisite analogues containing the benzylic amine function (Scheme 3).

Amide derivatives **3a−f** were obtained starting with Boc-protected amino acid **19**. Amidation was performed using HBTU or EDCI as the activating agents. HCl-mediated removal of the Boc group furnished the final analogues (Scheme 4).

Preparation of benzyl ether **15** commenced with protection of the oxindole nitrogen using SEM group. Chemoselective reduction of the ester group in **22** could be achieved by application of lithium borohydride. Williamson ether synthesis followed by the deprotection steps resulted in the formation of the desired product (Scheme 5). A target **16** with an all-carbon linker was accessed starting with Boc-protected amino aldehyde **21**. A sequence of Witting olefination, hydrogenation over palladium on carbon, and acid-promoted Boc deprotection furnished the final product (Scheme 6).

Preparation of the phenyl analogue **4** required utilization of a different Pictet−Spengler precursor. 3-(β-Aminophenethyl)-indole[44] was employed to this end. Analogous to the transformation described in Scheme 1, the Pictet−Spengler step was effected by treatment with formaldehyde in methanol. The basic amine was protected as Boc-carbamate, and the oxidative rearrangement was achieved by action of NBS.

Scheme 4. Synthesis of (3S,5′R)-2-Oxo-1,2-dihydrospiro[indole-3,3′-pyrrolidine]-5′-carboxamides 3a−f[a]

3a: R₁=H; R₂=Me
3b: R₁=R₂=Me
3c: R₁=R₂=H
3d: R₁=Me; R₂=tetrahydro-2H-pyran-4-yl
3e: R₁=H; R₂=benzyl
3f: R₁=H; R₂=tetrahydro-2H-pyran-4-yl
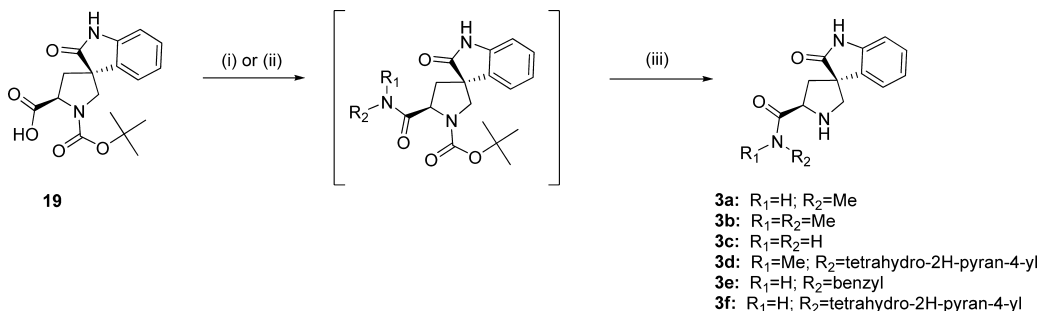
[a]Reagents and conditions: (i) HBTU/R₁R₂NH₂; (ii) EDCl/R₁R₂NH₂; (iii) 4 M HCl/dioxane.

Scheme 5. Synthesis of (3S,5′R)-5′-(Benzyloxymethyl)spiro[indoline-3,3′-pyrrolidin]-2-one 15[a]
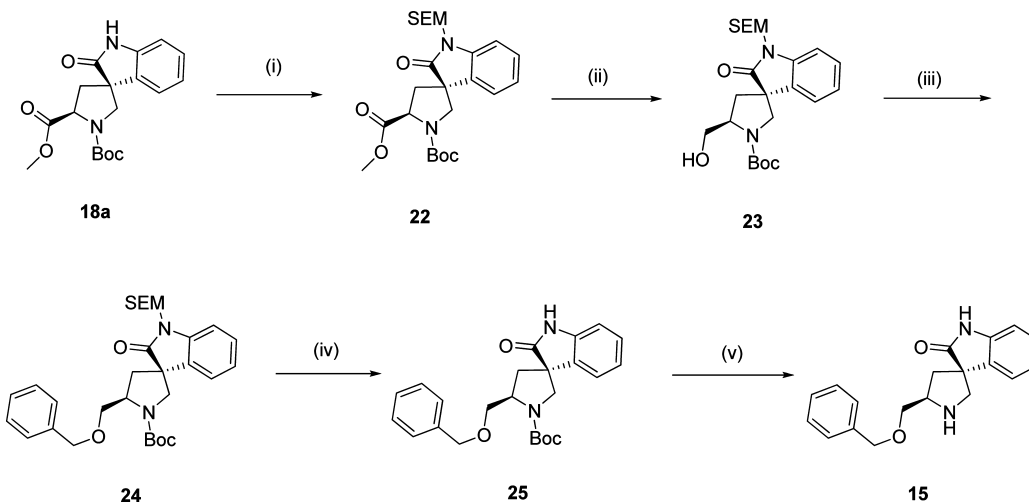
[a]Reagents and conditions: (i) t-BuOK/SEMCl/THF; (ii) LiBH₄/THF; (iii) BnBr/NaH; (iv) TBAF/THF; (v) HCl/dioxane/MeOH.

Scheme 6. Synthesis of (3S,5′S)-5′-(3-Phenylpropyl)-spiro[indoline-3,3′-pyrrolidin]-2-one 16[a]

[a]Reagents and conditions: (i) LiHMDS/phenethyltriphenylphosphonium bromide; (ii) H₂, Pd/C; (iii) HCl/dioxane/MeOH.

The intermediate enriched with the desired relative stereochemistry was isolated by column chromatography. Boc-removal using HCl afforded the requisite 5-phenyl substituted pyrrolidine derivative **4** as a 6:1 racemic mixture of diastereomers (Scheme 7).
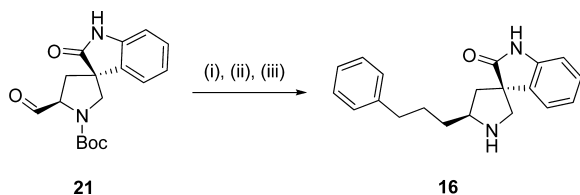
CONCLUSIONS

Development of viable BACE inhibitors historically has been difficult mainly due to the combination of property constraints imposed on potent aspartic protease inhibitors and a requirement for sufficient drug exposure levels in CNS. A variety of approaches are being utilized by academic and industry research groups to achieve this objective. FBDD represents a valuable opportunity and has already been met with considerable success in identifying new classes of BACE

inhibitors.[16−19,41,44,54] In our work, we utilized X-ray crystallography as a primary vehicle for hit identification.

Most BACE fragment screening efforts have historically resulted in the discovery of charged primary amines which interact directly with the catalytic Asp residues. Such ligands have the advantage of replacing the tightly bound catalytic water, normally situated between the charged carboxylates of Asp32 and Asp228, with an enthalpically favorable polar interaction with a positively charged NH₂ group. A notable exception to this is the tyrosine metabolite tyramine, first reported by Kuglstatter et al., in which the protonated primary amine of tyramine interacts with the catalytic water and only indirectly with the catalytic aspartates.[18] In the cases of the aminoquinolines and the isocytosines, as well as with the tyramine series, lead optimization proceeded primarily through optimization of contacts on the nonprime side of the BACE active site as reviewed by Kuglstatter and Hennig.[45] Like the aminoquinolines and isocytosines, the spiropyrrolidine series described here also displaces the catalytic water, replacing it with the (presumably) less favorable pyrrolidine NH interaction. We suggest that the relatively high ligand efficiency of **1** is likely due to the network of interactions which are established between the compound and both the catalytic aspartates and the flap residues (Figure 1). This network of interaction is highly specific, as reversal of the oxindole, which presumably would be allowed by a flip of the Gln73−Gly74 peptide bond back to a more "normal" configuration, results in

Scheme 7. Synthesis of (3S,5′R)-5′-Phenylspiro[indole-3,3′-pyrrolidin]-2(1H)-one 4[a]
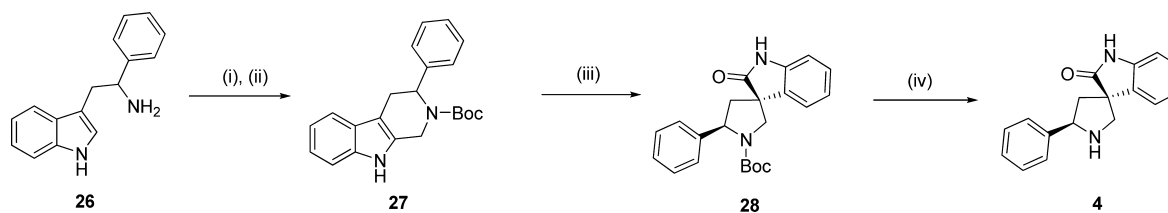

[a]Reagents and conditions: (i) HCHO/MeOH, 80 °C; (ii) Boc$_2$O/TEA; (iii) NBS/THF/H$_2$O/AcOH; (iv) 4 M HCl/dioxane.

a decrease in potency (data not shown). Furthermore, the rigid spirocycle clearly establishes the favorable geometry necessary for these interactions without necessitating an entropic penalty for ordering each of the hydrogen bonding groups. Unlike the aforementioned fragment lead series, the tight sequestration of the aromatic portion of compound **1** within the S1 subsite effectively precludes efforts to improve this series through modification on the nonprime side. One exception to this is the pyrrolidine 2 position (β face) which is clearly oriented toward the S2 pocket. However, inspection of the crystal structure of **1** overlaid with other inhibitor series which exploit this pocket suggested that effective exploration of this pocket would require a long flexible linker, which would presumably add significant mass, flexibility, and polarity to the template, attributes which generally are not desirable in brain penetrant drugs. Hence, all of the affinity optimization was conducted using the pyrrolidine 5 position as the primary growth vector.

The pyrrolidine group itself is not unprecedented as a general core for inhibitors of aspartyl proteases. Several examples of inhibitors of the related aspartyl protease, HIV protease, which utilize a pyrrolidine group as the primary interaction motif with the catalytic machinery, have been disclosed in recent years.[46−49] In these examples, the pyrrolidine ring sits somewhat deeper between the catalytic aspartates and does not deflect either of the carboxylates from coplanarity. Owing to the 2-fold symmetry of HIV-protease, which is an obligate homodimer, many of these compounds are perfectly symmetric and rely on interactions with the flap to increase potency. In contrast, **1** sits more deeply within the BACE S1 pocket and less so with respect to the catalytic machinery (Figure 10). As in the HIV-protease examples, the spirocyclic pyrrolidines described here also rely on interactions with the flap. BACE does not possess 2-fold symmetry, so the interactions as well as the optimization strategy are necessarily asymmetric.

As this manuscript was being finalized, a recent publication by Stachel et al. reported the discovery of a pyrrolidine-based BACE inhibitor via a high-concentration high-throughput screen.[50] These 3,4-disubstituted pyrrolidines bear a striking resemblance to those reported previously.[40] In contrast to our spiropyrrolidines, however, the pyrrolidine scaffold described by Stachel et al. was much more potent from the outset, albeit with a low LE value of 0.19.[50] The approach used in that paper utilized traditional medicinal chemistry SAR, rather than the heavy reliance upon crystallographic data used in the current manuscript, to drive ligand optimization efforts. The introduction of a spirocyclic tetrahydronapthlene to drive potency through interactions in the S1 pocket was only made at a late stage and resulted in a very lipophilic molecule with suboptimal physicochemical properties. The information provided by Stachel et al.[50] suggests several differences between the binding mode exhibited by their pyrrolidine scaffold and the spiropyrrolidines reported herein. First, the spiro fused
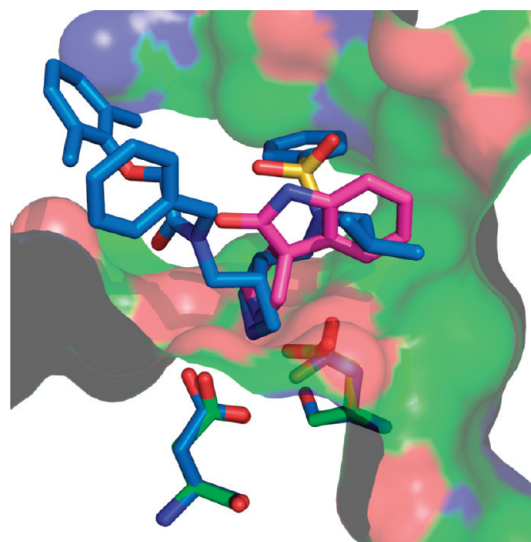
Figure 10. Overlay of an HIV protease pyrrolidine inhibitor (RCSB entry 1XL2) with **1**. The two crystal structures were superimposed upon the catalytic aspartates (HIVpr residue 25; BACE residues 32, 228). The color scheme is as in Figure 1, except for the carbon atoms of the HIV protease inhibitor, which are blue. The catalytic aspartic acids from both BACE (green carbon atoms) and HIV protease (blue carbon atoms) are depicted as sticks for reference. Alignment and figure were made with Pymol (Schrodinger, LLC).

tetrahydronaphthalene does not result in a substantial shift in the configuration of the catalytic aspartic acids in contrast to the orthogonal orientation observed in our series. Second, the liphophilic tetrahydronaphthalene does not appear to form stabilizing interactions with the flap, unlike the extensive network of hydrogen bonds observed in the spiro fused oxindoles. Finally, the large substituents in the starting scaffold reported by Stachel et al. induce large conformational changes in the prime side specificity pockets, especially in the vicinity of Tyr71. No such conformational changes are observed in the series reported in this manuscript.

A multidisciplinary approach was the key factor in our hit optimization efforts. Medicinal chemistry considerations were an integral part in the analysis of the binding mode, identification of the growth vectors, and assessing potential of this series for lead optimization efforts. X-ray crystallography and functional NMR assay allowed for facile SAR generation and confidence in interpretation of SAR trends for analogues spanning a wide potency range. In conclusion, we have discovered a novel structural motif capable of efficient BACE inhibition. Multidisciplinary analysis of the binding mode led to identification of a productive growth vector for potency optimization of **1**. It has been demonstrated that, for this scaffold, a potency improvement of practically 3 orders of

Table 4. X-Ray Statistics Data

	1	5	6	8	9	11	12	13	14
				(A) Data Collection					
space group	C222₁	C222₁	C222₁	C222₁	C222₁	C222₁	C222₁	C222₁	C222₁
Unit Cell	a = 74.8, b = 103.8, c = 99.6	a = 74.8, b = 103.9, c = 100.2	a = 74.7, b = 104.9, c = 101.5	a = 74.8, b = 103.6, c = 99.0	a = 74.6, b = 103.6, c = 98.7	a = 74.7, b = 104.0, c = 99.4	a = 74.5, b = 103.9, c = 98.5	a = 74.5, b = 103.9, c = 98.5	a = 74.5, b = 104.1, c = 99.6
resolution (Å) (high res)	46–1.71 (1.77–1.71)	38–1.80 (1.86–1.80)	30–2.50 (2.59–2.50)	50–1.94 (2.01–1.94)	49–2.00 (2.07–2.00)	50–2.00 (2.07–2.00)	50–1.95 (2.02–1.95)	50–2.73 (2.74–2.73)	50–1.95 (2.02–1.95)
completeness	98.7 (90.5)	99.4 (95.0)	99.5 (99.8)	99.4 (94.8)	93.3 (93.3)	99.2 (98.3)	95.8 (85.4)	100.0 (100.0)	96.1 (91.6)
R_{sym}^{a}	0.043 (0.417)	0.050 (0.356)	0.096 (0.533)	0.059 (0.439)	0.136 (0.622)	0.140 (0.597)	0.098 (0.745)	0.104 (0.604)	0.049 (0.180)
χ^2	0.99(1.76)	0.96(1.26)	1.00(1.29)	1.56(1.25)	0.96(1.13)	1.41(1.31)	1.24(1.02)		1.29(1.18)
redundancy	4.73 (3.81)	4.62 (3.48)	4.60(4.65)	4.65(4.2)	4.30(3.75)	4.6 (4.4)	4.2(3.5)	4.8(5.0)	4.8(3.8)
$I/\sigma(I)^{b}$	13.1(2.8)	12.5(3.0)	8.9(1.8)	31.2 (3.2)	5.0(1.3)	11.7(2.6)	13.7(1.3)	15.1(2.9)	304(6.8)
				(B) Refinement					
R_{work}^{c}	0.191	0.203	0.219	0.181	0.193	0.225	0.201	0.155	0.178
R_{free}^{c}	0.241	0.248	0.306	0.243	0.279	0.308	0.275	0.244	0.247
amino acid residues (no.)	394	394	394	394	394	394	394	394	394
waters (no.)	319	227	36	285	231	339	302	119	380
rmsd bond length (Å)	0.01	0.01	0.007	0.01	0.009	0.01	0.01	0.01	0.01
rmsd angle (deg)	1.22	1.4	0.87	1.27	1.16	1.02	1.11	1.2	1.28
average B (Å²)	24.3	24.3	30.5	24.3	23.2	18.7	25.5	40.9	17.2
Ramachandran	98.6	98.1	97.5	99.2	98.0	97.5	97.2	97.2	98.9
Ramachandran outliers (%)	1.4	1.9	2.5	0.8	2.0	2.5	2.8	2.8	1.1

$^{a}R_{sym} = \sum_{hkl} (|I_{hkl} - \langle I_{hkl}\rangle|)/\sum_{hkl} \langle I_{hkl}\rangle$, where I_{hkl} is the intensity of reflection hkl, and $\langle I_{hkl}\rangle$ is the average intensity of multiple observations. ^{b}Data for compounds 8, 11, 12, and 14 were processed using HKL2000. Hence $I/\sigma(I)$ is reported as $\langle I\rangle/\langle\sigma(I)\rangle$. $^{c}R_{work} = |\sum F_o - F_c|/\sum F_o$, where F_o and F_c are the observed and calculated structure factor amplitudes, respectively. R_{free} is the R-factor for a randomly selected 5% of reflections which were not used in the refinement.

magnitude was possible without significant deterioration of the ligand efficiency profile and in vitro properties predictive of brain penetration (RRCK permeability and efflux in MDR line). A number of productive interactions with residues in S1,′ S2′ pockets and with the flap region of BACE have been identified which could guide future work in search of ester isosteres en route to more potent analogues in this novel chemical series.

■ EXPERIMENTAL SECTION

X-Ray and Biophysics. *Crystallization of BACE.* Crystals of BACE were prepared as previously described.[31] Briefly, recombinant BACE lacking the pro-segment was concentrated to 10−13 mg/mL in 0.1 M sodium borate, pH 8.5. Crystallization was done by the vapor diffusion method, using 2 μL of protein solution and 2 μL of reservoir solution (30% PEG 200; 0.1 M sodium acetate, pH 5.2−5.4). Drops were microseeded 24 h post set up with 0.3−0.5 μL of seed stock made from a previously grown BACE crystal. Crystals generally grew to ∼0.1 × 0.1 × 0.05 mm³ in 2 weeks. The crystal form is C222₁, with a single molecule of BACE in the asymmetric unit, and diffracts to high resolution ($d_{min} < 2.0$ Å) with typical synchrotron X-ray exposure times (1−5 s/0.5° oscillation).

Preparation of Compounds. The fragment collection chosen for the X-ray-based fragment screen is a subset of the Pfizer Global Fragment Initiative (GFI).[30] This X-ray subset was comprised of 340 compounds selected for their shape and chemical diversity (30:30:40 acids/bases/neutrals), plated as mixtures of four compounds per well at 50 mM each compound in DMSO (85 mixtures in total). To enhance the likelihood of detecting very weakly binding compounds, the mixtures were concentrated 4× to 200 mM/compound by rotary evaporation and resuspension in neat DMSO. This concentration allowed for screening of the library at 20 mM per compound.

Soaking of Crystals. Soaking solutions were made by diluting the concentrated stock compound mixtures 1:10 with 30% PEG 200; 0.1 M sodium acetate pH 5.2. Crystals were transferred individually

from their mother drops to a 5 μL drop of soaking solution and allowed to equilibrate at 21 °C for ∼24 h. Following this equilibration, crystals were flash cooled for data collection by harvesting in rayon loops and plunging directly into liquid nitrogen.

Data Collection. X-ray diffraction data were collected at the Advanced Photon Source using the IMCA-CAT 17-BM beamline outfitted with a Mar CCD detector. All data sets were collected at a distance of 120 mm and a wavelength of 1.0 Å. For each crystal, a total of 120° of data were collected in 0.5° oscillations, generally yielding ∼100% complete data coverage at 4−5× redundancy for accurate scaling and outlier rejection. Data processing was performed using D*trek.[32] Compound mixtures which resulted in poor diffraction (d_{min} > 2.5 Å) were re-evaluated at 2 mM and 200 μM compound concentrations (1:100 and 1:1000 dilutions of the DMSO stock, respectively). Diffraction data statistics are reported in Table 4A.

Structure Solution. All data sets with $d_{min} \leq 2.5$ Å were refined using the program AUTOBUSTER,[33] using a rigid-body protocol for the first big cycle, followed by four big cycles of maximum entropy refinement using the GELLY refinement protocol. The initial model was a 1.5 Å crystal structure of apo BACE that was solved as part of an ongoing structure-based drug design effort. As we expected conformational variability in the "flap" region of BACE, residues 68−75 were excised from the model prior to refinement to minimize difficulty in interpretation of the $mF_o − dF_c$ σA-weighted difference maps. Binding of compounds to the BACE active site was assessed by visual inspection of the resulting difference maps using the program COOT.[51] Refinement statistics are reported in Table 4B.

NMR Saturation Transfer Difference (STD) Experiments. STD binding studies were carried out using 5 μM BACE and 250 μM ligand in a buffer consisting of 75 mM potassium phosphate at pH 7.0, 50 mM NaCl, and 0.02% sodium azide in 90% H_2O−10% ^2H_2O. Final DMSO concentration was 2.5%. STD experiments were acquired on a Bruker DRX600 spectrometer equipped with an inverse triple resonance 5 mm cryoprobe. STD spectra were collected at 20 °C with 512 scans, an irradiation frequency of 455 Hz, and time of 3 s and employing a Watergate 3−9−19 water suppression sequence. STD

competition experiments were conducted on ligands that had a positive STD signal by addition of 50 μM of a known HEA inhibitor (N-[(1S,2R)-1-[(3,5-difluorophenyl)methyl]-3-[[4-[3-(1,1-dimethylethyl)-phenyl]tetrahydro-2H-pyran-4-yl]amino]-2-hydroxypropyl]-acetamide[42]) to the original STD sample and repeating the experimental methodology. Reduction of signal intensity between the two spectra was indicative of binding in the known active site of BACE.

NMR ^{15}N−^{1}H TROSY Correlation Experiments. Binding studies were conducted on single compounds using a 60 μM ^{15}N isotopically labeled BACE solution in 75 mM potassium phosphate buffer at pH 7.0, 50 mM NaCl, and 0.02% sodium azide in 90% H_2O−10% ^2H_2O. Ligand concentration was 300−500 μM. ^{15}N−^{1}H TROSY spectra were acquired on a Bruker DRX600 spectrometer equipped with an inverse triple resonance 5 mm cryoprobe. TROSY data were collected using 2048 points in the direct dimension and 256 rows in the indirect dimension, 32 scans in each row at a temperature of 30 °C. Data was processed using FELIX software, and amide chemical shifts perturbations of active site residues related to the control spectrum were identified. The degree of chemical shift perturbation between an apo spectrum and a liganded spectrum for each of the 40 active site residues was calculated for each ligand and mapped against the X-ray structure of BACE with compound **1** bound.

Biolayer Interferrometry K_D determination using Octet. Experiments were performed on an Octet GK instrument (ForteBio). Streptavidin-coated FA tips were saturated with 0.015 μM biotinylated stat−val peptide.[53] Typical capture levels were between 0.2−0.3 nM within a row of eight tips. First, 500 nM BACE was precincubated with and without a series of several of several concentrations of compound and was then bound to the stat−val peptide for 5 min and allowed to dissociate for 1 min. All data was collected at 25 °C in 50 mM sodium acetate, pH 5.0, 150 mM NaCl, 0.05% polyoxyethylene sorbitant (surfactant P20 from GE Healthcare BioSciences), 1 mg/mL BSA, and 2−4% DMSO. Binding responses were processed by Biaeval (GE Healthcare) to zero, align and reference the data. Biaeval was also used to determine K_D values. Compound **1** binding affinity (K_D) was calculated by first determining the amount of free BACE that bound to the stat−val peptide[53] in the presence of compound and then plotting the [free BACE] vs [compound].

NMR Functional Activity Assay. The NMR BACE activity assay was developed using a modified substrate with the amino acid sequence NH-SEVNLAAEF-COOH. All BACE and peptide substrate solutions were prepared in 90% ^1H_2O/10% ^2H_2O and were buffered with 50 mM deuterated sodium acetate pH 5.0 containing 50 mM NaCl, 0.02% sodium azide, and 0.008% Triton X-100. Then 10.6 μL of a DMSO-d_6 compound solution was added to 320 μL of a 48 μM peptide substrate stock solution. The enzymatic reaction was initiated by adding 200 μL of a 250 nM BACE solution in the same buffer, and the reaction was incubated for 30 min at ambient temperature. The final reaction conditions consisted of 100 nM BACE and 29 μM peptide substrate. The reaction was quenched with 20 μL of an 550 μM solution of a known potent hydroxyethylamine (HEA) inhibitor, N-[(1S,2R)-1-[(3,5-difluorophenyl)methyl]-3-[[4-[3-(1,1-dimethylethyl)phenyl]-tetrahydro-2H-pyran-4-yl]amino]-2-hydroxypropyl]-acetamide.[42] NMR data were collected at on a Bruker DRX600 spectrometer equipped with an inverse triple resonance 5 mm cryoprobe. A 1D ^{1}H NMR spectrum with 512 scans was collected at 20 °C for each sample using a Watergate 3−9−19 water suppression sequence. The extent of product formation was monitored by comparing the intensity of the alanine methyl resonance of the cleaved product at 1.4 ppm or the amide resonance at 8.3 ppm to control wells without inhibitor added. Percent inhibition at single or multiple concentration(s) was recorded. IC_{50} value was obtained by curve fitting using Microcal Origin software.

Biology. *Cell-Free Biochemical Assay.* BACE activity was measured using an in-house generated antibody, p1007, that specifically recognizes the new APP$_{swe}$ C-terminus created after cleavage by BACE. Rabbits were immunized with the peptide NH$_2$-EISEVNL-COOH conjugated to keyhole limpet hemacyanin. Concentrated conditioned media from cells secreting human recombinant soluble BACE was titrated to provide a source of BACE enzyme. The reaction is initiated by the addition of soluble BACE enzyme to a mixture containing 0.05 M sodium acetate (pH 4.5), compound inhibitor, 2% DMSO, and 3 μM APP substrate (K(biotin)RGLTTRPGSGLTNIKTEEISEVNLDAEFRHDSGA, American Peptide). The reaction is incubated at 37 °C for 1 h and quenched by the addition of an equivalent volume of 0.1 M Tris, pH 8.0. Cleaved product is measured via a TMB-ELISA with streptavidin coated capture plates (Greiner Bio-One), p1007 reporter (Pfizer), and tertiary anti rabbit-HRP (GE Healthcare UK).

Chemistry. *General Methods.* NMR spectra were obtained on Varian INOVA spectrometers (300, 400, or 500 MHz). Chemical shifts are expressed in δ (ppm) units relative to solvent residual peak, and peak multiplicity are expressed as follows: singlet (s), doublet (d), doublet of doublets (dd), triplet (t), multiplet (m), broad singlet (br s), broad multiplet (br m). Unless otherwise indicated, all mass spectrometric measurements were performed using a Micromass Platform ZQ (Waters, Manchester, UK) mass spectrometer operated in positive electrospray ionization mode using 5−100% acetonitrile in water gradient containing 0.1% TFA on a Phenomenex 5 μm C18 4.6 mm × 50 mm Gemini column.

All reactions were carried out under nitrogen atmosphere or in sealed vials. Dry solvents and reagents were of commercial quality and were used as purchased. Except if indicated otherwise, reactions were magnetically stirred and monitored by thin-layer chromatography using Merck silica gel 60 F254 by fluorescence quenching under UV light or by LC/MS detection. In addition, TLC plates were stained using phosphomolybdic acid or potassium permanganate stain. Chromatographic purification of products (flash chromatography) was performed on Isco Combiflash systems using Redisep columns and ethyl acetate/heptanes gradients. Concentration under reduced pressure was performed by rotary evaporation at 40 °C at the appropriate pressure unless otherwise stated. The purity of the compounds reported in the manuscript was established through HPLC-MS methodology. All the compounds reported in the manuscript have a purity >95% unless noted otherwise.

(3S)-Spiro[indole-3,3′-pyrrolidin]-2(1H)-one (1). Benzyl (3S)-2-oxo-1,2-dihydro-1′H-spiro[indole-3,3′-pyrrolidine]-1′-carboxylate was prepared from 2,3,4,9-tetrahydro-1H-β-carboline according to published procedures (WO2006/090261).

A solution of benzyl (3S)-2-oxo-1,2-dihydro-1′H-spiro[indole-3,3′-pyrrolidine]-1′-carboxylate (300 mg, 0.930 mmol) in methanol (50 mL) was purged with nitrogen, charged with 20% Pd(OH)$_2$ (30 mg), and hydrogenated on a Parr shaker at 50 psi until complete as determined by TLC. The catalyst was filtered away and the solvents removed on a rotary evaporator under reduced pressure to afford **1** (175 mg, 100%) as a white solid. ^{1}H NMR (400 MHz, methanol-d_4) δ 7.30 (d, J = 7.41 Hz, 1H), 7.19 (t, J = 7.61 Hz, 1H), 7.01 (t, J = 7.42 Hz, 1H), 6.88 (d, J = 7.81 Hz, 1H), 3.30−3.50 (m, 3H), 3.17 (d, J = 11.71 Hz, 1H), 2.29 (td, J = 6.51, 12.93 Hz, 1H), 2.14 (td, J = 7.12, 13.46 Hz, 1H). MS (ES+) *m/z*: 189.1.

(3S,5′R)-5′-[(Benzylamino)methyl]spiro[indole-3,3′-pyrrolidin]-2(1H)-one (2a). A solution of lithium borohydride (1.0 M in THF, 4.8 mL, 9.6 mmol was added dropwise under nitrogen to a stirred solution of **5** (1.11 g, 3.20 mmol) in THF (10 mL) at room temperature. After 3 h, the reaction was quenched carefully by the dropwise addition of 1N HCl and ethyl acetate (20 mL). The aqueous phase was removed and extracted with ethyl acetate (2 × 10 mL), and the combined organic phases were washed with saturated NaHCO$_3$ (10 mL) and brine. The organic phase was dried over MgSO$_4$, filtered, and concentrated at reduced pressure to give 791 mg of white foam. This crude alcohol was purified by flash chromatography on 40 g silica gel using 1:1 ethyl acetate/heptanes eluent to afford 661 mg (2.08 mmol, 65%) of **20** as a white solid. ^{1}H NMR (400 MHz, methanol-d_4) δ 7.15−7.34 (m, 2H), 6.85−7.05 (m, 6H), 4.23 (dd, J = 3.52, 8.40 Hz, 2H), 3.81−3.94 (m, 2H), 3.63−3.79 (m, 4H), 3.39−3.58 (m, 2H), 2.40−2.61 (m, 2H), 2.03−2.18 (m, 2H). MS (ES+) *m/z*: 318.9.

Dess−Martin reagent (0.3 M in DCM, 607 μL, 0.18 mmol) was added to a solution of **20** (555 mg, 0.17 mmol) in DCM (1 mL). After 1 h at room temperature, the reaction was quenched with saturated

aqueous NaHCO$_3$ (2 mL) and 300 mg solid Na$_2$S$_2$O$_3$·5H$_2$O. The organic phase was dried (MgSO$_4$), filtered, and concentrated at reduced pressure to afford **21** (55 mg, 100%) as an amber oil which was carried on directly. ^{1}H NMR (400 MHz, chloroform-*d*) δ 9.70 (dd, *J* = 2.05, 14.94 Hz, 1H), 7.21−7.28 (m, 4H), 7.12−7.19 (m, 1H), 7.04−7.09 (m, 1H), 6.90 (d, *J* = 7.62 Hz, 1H), 2.43−2.50 (m, 1H), 2.31−2.40 (m, 1H), 1.38−1.52 (m, 9H). MS (ES+) *m/z*: 261.3.

Sodium triacetoxyborohydride (34 mg, 0.16 mmol) was added in one portion to a stirred solution of **21** (46 mg, 0.14 mmol) and benzylamine (18 mg, 0.16 mmol) in DCM (1 mL) at room temperature. After 16 h, the reaction was diluted with DCM (4 mL), washed with 5% NaHCO$_3$, and dried (MgSO$_4$). Solvent was removed under reduced pressure to afford the crude amine intermediate (52 mg) as an amber oil, which was purified by reverse phase HPLC to afford the clean intermediate (10.6 mg, 18%) as a white solid. ^{1}H NMR (400 MHz, methanol-*d*$_4$) δ 7.41−7.56 (m, 6H), 7.22−7.28 (m, 1H), 7.07−7.11 (m, 1H), 6.99−7.06 (m, 1H), 6.94 (d, *J* = 7.81 Hz, 1H), 4.57 (d, *J* = 6.05 Hz, 1H), 4.39 (d, *J* = 12.89 Hz, 1H), 4.20 (d, *J* = 12.89 Hz, 1H), 3.74 (d, *J* = 11.52 Hz, 1H), 3.58−3.65 (m, 1H), 3.53 (dd, *J* = 8.89, 12.99 Hz, 1H), 3.31−3.40 (m, 1H), 2.41 (dd, *J* = 8.20, 13.09 Hz, 1H), 2.16 (dd, *J* = 8.01, 13.28 Hz, 1H), 1.45 (s, 10H). MS (ES+) *m/z*: 408.6.

The Boc-protected pyrrolidine (10.6 mg, 0.0203 mmol) from the previous step was treated with 4 M HCl in dioxane (1 mL) and stirred at room temperature for 90 min. The reaction was concentrated under reduced pressure to afford **2a** (6.9 mg, 100%) as a white solid. ^{1}H NMR (400 MHz, methanol-*d*$_4$) δ 7.56−7.63 (m, 2H), 7.43−7.51 (m, 4H), 7.25−7.33 (m, 1H), 7.05−7.15 (m, 1H), 6.94 (d, *J* = 7.81 Hz, 1H), 4.52−4.65 (m, 1H), 4.35 (s, 2H), 3.60−3.84 (m, 4H), 2.65 (dd, *J* = 8.69, 13.97 Hz, 1H), 2.37−2.48 (m, 1H). MS (ES+) *m/z*: 308.5.

(3S,5′R)-5′-({[3-(Trifluoromethyl)benzyl]amino}methyl)spiro-[indole-3,3′-pyrrolidin]-2(1H)-one (2b). Dess−Martin periodinane (0.3 M in DCM, 910 μL) was added to a solution of **20** (51 mg, 0.14 mmol) in DCM (1 mL). The resulting yellow−green solution was stirred at room temperature for 2.5 h, washed with 5% aqueous sodium bicarbonate (2 mL), 5% aqueous sodium thiosulfate (2 mL), and dried over Na$_2$SO$_4$. The solvent was removed to afford **21** as a brown oil, which was used immediately without further purification.

Sodium triacetoxyborohydride (76 mg, 0.36 mmol) was added to a solution of **21** and 3-(trifluoromethyl)benzylamine (21.5 μL, 0.15 mmol) in DCE (2 mL). After 18 h at room temperature, the reaction was washed with 5% aqueous sodium bicarbonate (2 mL). The organic phase dried by loading onto a Varian ChemElut (Hydromatrix) cartridge (6 mL, 1 g sorbent), eluting after 3 min into a tared vial with DCE (3 × 2 mL). The crude material thus obtained was purified by silica gel flash chromatography (0−10% MeOH/DCE) to afford the intermediate (50 mg, 77%) as a cloudy brown oil. ^{1}H NMR (400 MHz, CDCl$_3$) δ 7.66−7.72 (m, 1H), 7.47−7.64 (m, 3H), 7.30 (d, *J* = 7.03 Hz, 1H), 7.22−7.27 (m, 1H), 7.00−7.10 (m, 2H), 6.94 (d, *J* = 8.4 Hz, 1H), 4.52 (br s, 1H), 3.95 (d, *J* = 13.3 Hz, 2H), 3.75−3.80 (m, 1H), 3.67 (t, *J* = 12.3 Hz, 2H), 3.17 (br s, 2H), 2.26−2.37 (m, 2H), 1.54−1.58 (m, 1H), 1.39−1.49 (m, 9 H). MS (ES+) *m/z*: 475.9.

A solution of the Boc-protected pyrrolidine (47.7 mg, 0.100 mmol) in 4 M HCl/dioxane (4.0 mL) was stirred at room temperature for 1 h. The reaction was reduced in vacuo until a brown precipitate separated from the pale-yellow mother liquor. This was collected and dried to afford **2b** as a tan solid (27.5 mg, 67%). ^{1}H NMR (400 MHz, DMSO-*d*$_6$) δ 10.80 (s, 1H), 9.76 (br s, 1H), 8.05 (s, 1H), 7.93 (d, *J* = 7.42 Hz, 1H), 7.81 (d, *J* = 7.81 Hz, 1H), 7.71 (t, *J* = 8.01 Hz, 1H), 7.62 (d, *J* = 7.62 Hz, 1H), 7.27 (td, *J* = 1.27, 7.76 Hz, 1H), 6.98−7.10 (m, 1H), 6.90 (d, *J* = 7.42 Hz, 1H), 4.38 (br s, 1H), 3.65 (br s, 2H), 3.49 (br s, 5H), 2.37−2.45 (m, 1H), 2.24−2.36 (m, 1H). MS (ES+) *m/z*: 376.0.

General Procedure for Boc-Deprotection. A solution of Boc-intermediate in 4 M HCl in dioxane (1 mL/20 mg) was stirred at room temperature for 1.5 h, whereupon the solvent was removed by evaporation and the final product dried under high vacuum to a constant weight. If the material was of insufficient purity, it was purified as indicated.

(3S,5′R)-N-Methyl-2-oxo-1,2-dihydrospiro[indole-3,3′-pyrroli-dine]-5′-carboxamide (3a). HBTU (135 mg, 0.356 mmol) and TEA

(33 mg, 0.33 mmol) were added to a solution of **19** (100 mg, 0.301 mmol) in DCM (1 mL) at room temperature. After 30 min, methylamine (2.0 M in methanol, 300 μL, 0.60 mmol) was added and stirring was continued for 1 h. The reaction was diluted with DCM (1 mL), washed with aqueous 5% NaHCO$_3$ (2 mL), and dried (MgSO$_4$). Filtration and removal of solvent under reduced pressure afforded the crude amide as a yellow oil. Flash chromatography on silica gel (40 g) with a 50−100% ethyl acetate/heptane gradient afforded the Boc-protected amide intermediate (73 mg, 70%) as a white foam. ^{1}H NMR (400 MHz, methanol-*d*$_4$) δ 7.17−7.30 (m, 1H), 6.98−7.10 (m, 2H), 6.94 (d, *J* = 7.81 Hz, 1H), 4.44−4.66 (m, 1H), 3.71 (td, *J* = 10.72, 21.73 Hz, 2H), 2.72−2.83 (m, 3H), 2.23−2.48 (m, 2H), 1.37−1.51 (m, 9H). MS (ES+) *m/z*: 346.4.

The Boc-protected pyrrolidine (54 mg, 0.16 mmol) from the previous step was deprotected according to the general method above to afford **3a** (45 mg, 100%) as a white foam. ^{1}H NMR (400 MHz, methanol-*d*$_4$) δ 7.45 (td, *J* = 0.66, 7.47 Hz, 1H), 7.30 (dt, *J* = 1.27, 7.76 Hz, 1H), 7.06−7.15 (m, 1H), 6.91−6.98 (m, 1H), 4.70−4.78 (m, 1H), 3.77 (d, *J* = 12.31 Hz, 1H), 3.58 (d, *J* = 11.91 Hz, 1H), 2.78−2.84 (m, 3H), 2.62 (dd, *J* = 8.40, 13.48 Hz, 1H), 2.48 (dd, *J* = 9.57, 13.48 Hz, 1H). MS (ES+) *m/z*: 246.3.

(3S,5′R)-N,N-Dimethyl-2-oxo-1,2-dihydrospiro[indole-3,3′-pyrro-lidine]-5′-carboxamide (3b). HBTU (66 mg, 0.17 mmol) and TEA (17 mg, 0.7 mmol) were added to a solution of **19** (48 mg, 0.14 mmol) in DCM (1 mL) at room temperature. After 30 min, dimethylamine (40% aqueous solution, 36 μL, 0.29 mmol) was added and stirring was continued for 1 h. The reaction was diluted with DCM (1 mL), washed with aqueous 5% NaHCO$_3$ (2 mL), and dried (MgSO$_4$). Filtration and removal of solvent under reduced pressure afforded the crude amide as a white foam. Flash chromatography on silica gel (12 g) with a 50−100% ethyl acetate/heptane gradient afforded the Boc-protected amide intermediate (40 mg, 77%) as a white foam. ^{1}H NMR (400 MHz, methanol-*d*$_4$) δ 7.21−7.29 (m, 1H), 7.09−7.20 (m, 1H), 7.00−7.07 (m, 1H), 6.91−6.96 (m, 1H), 5.07 (dd, *J* = 7.91, 9.47 Hz, 1H), 3.71−3.78 (m, 1H), 3.59−3.69 (m, 1H), 3.12 (d, *J* = 5.27 Hz, 3H), 2.98 (d, *J* = 5.66 Hz, 3H), 2.25−2.48 (m, 2H), 1.44 (d, *J* = 9.38 Hz, 9H). MS (ES+) *m/z*: 360.5.

The Boc-protected pyrrolidine (14 mg, 0.038 mmol) from the previous step was deprotected according to the general method above to afford **3b** (7.5 mg, 100%) as a white foam. ^{1}H NMR (400 MHz, methanol-*d*$_4$) δ 7.48−7.56 (m, 1H), 7.26−7.34 (m, 1H), 7.08−7.14 (m, 1H), 6.94 (d, *J* = 7.81 Hz, 1H), 5.13 (t, *J* = 9.08 Hz, 1H), 3.79 (d, *J* = 11.91 Hz, 1H), 3.60−3.64 (m, 1H), 3.03 (d, *J* = 6.45 Hz, 6H), 2.86 (dd, *J* = 9.38, 13.67 Hz, 1H), 2.41 (dd, *J* = 8.59, 13.67 Hz, 1H). MS (ES+) *m/z*: 260.4.

(3S,5′R)-2-Oxo-1,2-dihydrospiro[indole-3,3′-pyrrolidine]-5′-car-boxamide (3c). EDC (91 mg, 0.48 mmol) was added to a solution of **19** (150 mg, 0.45 mmol) and HOBt (92 mg, 0.68 mmol) in THF (3 mL). After 50 min at room temperature, concd NH$_4$OH (300 μL) was added slowly and the reaction was stirred for 48 h at room temperature. Saturated aqueous ammonium chloride (30 mL) was added, and the aqueous solution was extracted with ethyl acetate (3 × 15 mL). The organic phases were combined, dried (Na$_2$SO$_4$), and concentrated to a pale-yellow sticky solid. This was dried under high vacuum to afford the Boc-protected amide (118 mg, 79%), which was carried on without further purification. ^{1}H NMR (400 MHz, DMSO-*d*$_6$) δ 10.65 (s, 1H), 7.47−7.56 (m, 1H), 7.24 (td, *J* = 1.56, 7.52 Hz, 1H), 7.10−7.17 (m, 1H), 6.95−7.05 (m, 2H), 6.87−6.94 (m, 1H), 4.36−4.50 (m, 1H), 3.45−3.63 (m, 2H), 2.14−2.25 (m, 2H), 1.32−1.46 (m, 9H) (shows mixture of rotational isomers). MS (ES+) *m/z*: 331.9.

Deprotection according to the general method afforded **3c** (67%) as a white solid after reverse-phase preparative LC/MS (Phenomenex Gemini C18 21.2 mm × 150 mm, 5 μm, 95%H$_2$O/5%MeCN linear gradient to 5%H$_2$O/95%MeCN with ammonium hydroxide 0.1% modifier). ^{1}H NMR (400 MHz, DMSO-*d*$_6$) δ 10.42 (br s, 1H), 7.44−7.51 (m, 1H), 7.36 (dd, *J* = 0.59, 7.42 Hz, 1H), 7.18 (td, *J* = 1.27, 7.67 Hz, 1H), 7.12 (d, *J* = 2.54 Hz, 1H), 6.96 (td, *J* = 1.17, 7.52 Hz, 1H), 6.84 (d, *J* = 7.81 Hz, 1H), 3.95 (t, *J* = 8.40 Hz, 1H), 3.10 (d, *J* = 11.33 Hz, 1H), 2.91 (d, *J* = 11.33 Hz, 1H), 2.08−2.18 (m, 2H). MS (APCI+) *m/z*: 232.2.

(3S,5′R)-N-Methyl-2-oxo-N-(tetrahydro-2H-pyran-4-yl)-1,2-dihydrospiro[indole-3,3′-pyrrolidine]-5′-carboxamide (3d). HBTU (64 mg, 0.20 mmol) was added to a solution of **19** (52 mg, 0.16 mmol) and *N*-methyltetrahydro-2*H*-pyran-4-amine (37 mg, 0.32 mmol) in DMF (1 mL). After 18 h at room temperature, the reaction was diluted with 10 mL of ethyl acetate and washed with 2 mL each of 5% sodium bicarbonate, water, 15% citric acid, and brine. The organic phase was dried (Na_2SO_4) and concentrated to afford crude Boc-protected intermediate. Column chromatography (0−100% ethyl acetate/heptane gradient) afforded Boc-protected intermediate (9.7 mg, 14%) as a cloudy oil. ¹H NMR (400 MHz, CDCl₃) δ 8.51−8.60 (m, 1H), 7.25−7.31 (m, 1H), 7.15 (d, J = 7.4 Hz, 1H), 7.03−7.10 (m, 1H), 6.94−7.00 (m, 1H), 4.99−5.11 (m, 1H), 4.89 (dd, J = 8.20, 8.98 Hz, 1H), 4.76 (d, J = 9.57 Hz, 1H), 3.99−4.08 (m, 2H), 3.75−3.92 (m, 2H), 3.34 −3.56 (m, 2H), 2.90−2.97 (m, 3H), 2.45−2.55 (m, 1H), 2.30−2.39 (m, 1H), 1.72−1.87 (m, 1H), 1.53−1.71 (m, 2 H), 1.43−1.49 (m, 9 H). MS (ES+) *m/z*: 429.9.

Deprotection according to the general method afforded **3d** (99%) as an off-white solid. ¹H NMR (400 MHz, DMSO-*d₆*) δ 10.76 (s, 1H), 7.64 (t, J = 8.30 Hz, 1H), 7.26−7.31 (m, 1H), 7.07 (q, J = 7.75 Hz, 1H), 6.90 (d, J = 7.81 Hz, 1H), [5.17 (t, J = 8.89 Hz) and 5.05 (t, J = 9.18 Hz), 1H total, rotational isomers], 3.92 (dd, J = 4.8, 10.8 Hz, 2H), 3.60−3.65 (m, 1H), 3.57 (s, 4H), 3.37−3.50 (m, 2H), [2.83 (s) and 2.86 (s), 3H total, rotational isomers], 2.67−2.81 (m, 1H), 2.18−2.28 (m, 1H), 1.70−1.83 (m, 1H), 1.44−1.52 (m, 2 H). MS (ES+) *m/z*: 329.9.

(3S,5′R)-N-Benzyl-2-oxo-1,2-dihydrospiro[indole-3,3′-pyrrolidine]-5′-carboxamide (3e). HBTU (50 mg, 0.13 mmol) and TEA (19 μL, 0.13 mmol) were added to a suspension of **19** in DCM (2 mL). After 30 min at room temperature, benzylamine (24 μL, 0.22 mmol) was added and the reaction was stirred at room temperature overnight. The reaction was diluted with 1 mL DCM, washed with 5% NaHCO₃ (2 mL), dried (Na₂SO₄), and concentrated to afford crude intermediate as a colorless oil. Column chromatography (0−100% ethyl acetate/heptane gradient) afforded the desired Boc-intermediate (43 mg, 93%) as a white solid. MS (EI+) *m/z*: 422.4.

Deprotection according to the general method afforded **3e** (90%) as an off-white solid. ¹H NMR (400 MHz, DMSO-*d₆*) δ 10.78 (s, 1H), 9.06 (t, J = 5.96 Hz, 1H), 7.48−7.58 (m, 1H), 7.32−7.38 (m, 2H), 7.24−7.32 (m, 4H), 7.06 (td, J = 1.17, 7.52 Hz, 1H), 6.87−6.94 (m, 1H), 4.75 (dd, J = 7.32, 11.04 Hz, 1H), 4.39 (d, J = 5.86 Hz, 2H), 3.62 (d, J = 12.11 Hz, 1H), 3.46−3.52 (m, 1H), 2.52−2.56 (m, 1H), 2.28 (dd, J = 11.13, 13.09 Hz, 1H). MS (ES+) *m/z*: 322.3

(3S,5′R)-2-Oxo-N-(tetrahydro-2H-pyran-4-yl)-1,2-dihydrospiro[indole-3,3′-pyrrolidine]-5′-carboxamide (3f). EDC (37 mg, 0.19 mmol) was added to a solution of **19** (52 mg, 0.16 mmol) and tetrahydro-2*H*-pyran-4-amine (20 mg, 0.19 mmol) in DCM (1 mL) and stirred for 48 h at room temperature. The reaction was diluted with 2 mL of DCM, washed with water (3 × 1 mL), and dried over Na₂SO₄. Removal of the solvent afforded crude intermediate as a cloudy oil. Column chromatography (50−100% ethyl acetate/heptane gradient) afforded the Boc-intermediate (14 mg, 21%) as a cloudy oil. ¹H NMR (400 MHz, CDCl₃) δ 8.22−8.53 (m, 1H), 7.16−7.28 (m, 1H), 6.96−7.07 (m, 2H), 6.83−6.97 (m, 1H), 6.72 (br s, 1H), 4.35−4.78 (m, 1H), 3.86−4.08 (m, 2H), 3.61−3.87 (m, 1H), 3.35−3.57 (m, 2H), 2.84 (br s, 1H), 2.45−2.68 (m, 1H), 2.33 (br s, 1H), 1.71−1.99 (m, 4H), 1.33−1.60 (m, 10H). MS (ES+) *m/z*: 415.9.

Deprotection according to the general method afforded **3f** (100%) as an off-white solid. ¹H NMR (400 MHz, DMSO-*d₆*) δ 10.73 (s, 1H), 8.51 (d, J = 7.81 Hz, 1H), 7.48 (d, J = 7.81 Hz, 1H), 7.25 (td, J = 1.17, 7.72 Hz, 1H), 7.03 (td, J = 1.07, 7.57 Hz, 1H), 6.88 (d, J = 7.42 Hz, 1H), 4.59 (dd, J = 7.23, 11.13 Hz, 1H), 3.78 (tt, J = 3.81, 11.33 Hz, 3H), 3.57 (d, J = 12.11 Hz, 1H), 3.45 (d, J = 11.91 Hz, 1H), 3.33−3.41 (m, 2H), 2.38−2.44 (m, 1H), 2.19 (dd, J = 11.23, 12.99 Hz, 1H), 1.71 (t, J = 15.43 Hz, 2H), 1.24−1.46 (m, 2H). MS (ES+) *m/z*: 316.0.

(5′-Phenylspiro[indole-3,3′-pyrrolidin]-2(1H)-one (4). Formaldehyde solution (17 μL, 0.22 mmol) was added to a stirred mixture of 2-(1*H*-indol-3-yl)-1-phenylethanamine (**26**, CAS 1148−06−7) in methanol (1 mL). After 10 min at 80 °C, a precipitate formed whereupon the reaction was cooled to room temperature. Solvent was

removed under reduced pressure, and the resulting solid was used in the next step without further purification.

Triethylamine (51 mg, 0.51 mmol) and di-*tert*-butyl dicarbonate (42 mg, 0.19 mmol) were added to a mixture of the crude tetrahydro-β-carboline prepared above (42 mg, 0.17 mmol) in THF (1 mL) and water (0.25 mL). After 2 h at room temperature, the solvent was removed under reduced pressure and the residue partitioned between DCM (2 mL) and 5% aqueous NaHCO₃ (2 mL). The organic phase was dried over Na₂SO₄, filtered, and concentrated under reduced pressure to afford crude Boc-protected tetrahydro-β-carboline (59 mg 0.17 mmol) as an amber foam, which was used directly in the next reaction

N-Bromosuccinimide (30 mg, 0.17 mmol) was added to a solution of the Boc-tetrahydro-β-carboline **27** prepared above (59 mg, 0.17 mmol) in THF/water/HOAc (1 mL/0.5 mL/0.1 mL) at 0 °C. After 1 h at 0 °C, the reaction was diluted with DCM (2 mL) and saturated NaHCO₃ (2 mL). The organic phase was dried (Na₂SO₄), filtered, and concentrated under reduced pressure. Column chromatography on silica (12 g) with (1:3 ethyl acetate/heptane) afforded the rearrangement intermediate (30 mg, 48%) as a pale-yellow solid which was used directly in the next step.

The Boc-protected 5′-phenylpyrrolidine **28** (25 mg, 0.069 mmol) prepared above was dissolved in methanol (1 mL) and treated with 4 M HCl in dioxane (1 mL). After 1 h, the solvent was removed to afford **4** (21 mg, 100% yield) as a tan solid. NOE experiments indicated a 6:1 mixture of diastereomers with (3S,5′R) relative stereochemistry as the major isomer. ¹H NMR (400 MHz, methanol-*d₄*) δ 7.57−7.62 (m, 2H), 7.42−7.57 (m, 3H), 7.26−7.34 (m, 1H), 7.05−7.22 (m, 2H), 6.91−6.99 (m, 1H), 5.37 (dd, J = 6.54, 11.82 Hz, 1H), 3.73−3.89 (m, 2H), 2.64−2.84 (m, 2H). MS (ES+) *m/z*: 265.3.

Methyl (3S,5′R)-2-Oxo-1,2-dihydrospiro[indole-3,3′-pyrrolidine]-5′-carboxylate (5). A solution of **18a** (141 mg, 0.407 mmol) in THF (1 mL) was treated with 4 M HCl in dioxane (1 mL). After 1 h, the solvent was removed under reduced pressure and the residue partitioned between DCM (10 mL) and 5% aqueous NaHCO₃ (10 mL). The organic phase was dried over MgSO₄, filtered, and concentrated at reduced pressure to afford **5** (52 mg, 50%) as a viscous colorless oil. ¹H NMR (400 MHz, methanol-*d₄*) δ 7.31−7.35 (m, 1H), 7.16−7.23 (m, 1H), 6.98−7.06 (m, 1H), 6.85−6.91 (m, 1H), 4.21 (dd, J = 7.52, 8.50 Hz, 1H), 3.76 (s, 3H), 3.36 (d, J = 11.52 Hz, 1H), 3.02 (d, J = 11.52 Hz, 1H), 2.33−2.46 (m, 2H). MS (ES+) *m/z*: 246.9.

Ester Formation: Method A (Activated Ester). A solution of DCC (1.0 equiv) and DMAP (10 mol %) in dichloromethane (0.25 M with respect to DCC) was added to a stirring suspension of **19** (1 equiv) and the appropriate alcohol (1.1 equiv) in dichloromethane (0.25 M with respect to **19**) at 0 to 5 °C (external temperature). A white precipitate formed as the resulting solution was allowed to come to room temperature over 2 h. The reaction was diluted with DCM, agitated on a vortexer, and filtered through Celite. The filter cake was washed with dichloromethane (2 mL), the combined filtrates were washed with saturated aqueous sodium bicarbonate solution (2 mL), and the lower organic layer was passed through a phase separation cartridge. After removal of the solvent, the resulting Boc-protected ester intermediate was dissolved in methanol (500 μL) and treated with HCl in 1,4-dioxane (4 M solution, 10 equiv). After 3−5 h at room temperature, the reaction mixture was concentrated to near dryness and purified by reverse-phase preparative chromatography to afford the desired products.

Ester Formation: Method B (Mixed Anhydride). Triethylamine (5 equiv) and 2,4,6-trichlorobenzoyl chloride (1.1 equiv) were added to a solution of **19** (1.0 equiv) in DCM (0.23 M with respect to **19**). After 30 min at room temperature, the appropriate alcohol reactant (2.3 equiv) was added followed by DMAP (1 equiv). The resulting mixture was stirred at room temperature for 1−5 h and loaded directly onto a pre-equilibrated normal-phase flash column for purification (ethyl acetate/heptane gradient). After removal of the solvent, the resulting Boc-protected ester intermediate was dissolved in methanol (0.045 M) and treated with HCl in 1,4-dioxane (4 M solution, 42 equiv). After 2−5 h, the solvent was removed in vacuo and the residue dried under high vacuum to afford the ester product as the

monohydrochloride salt. If the material was of insufficient purity, it was purified by reverse-phase preparative chromatography.

Tetrahydro-2H-pyran-4-yl (3S,5′R)-2-Oxo-1,2-dihydrospiro-[indole-3,3′-pyrrolidine]-5′-carboxylate (6). Prepared by method B from **19** (48 mg, 0.14 mmol) and tetrahydro-4*H*-pyran-4-ol (29 mg, 0.29 mmol) to afford **6** (15 mg, 32% over both steps) as a pale-yellow solid. ¹H NMR (400 MHz, methanol-*d*₄) δ 7.44 (d, *J* = 7.23 Hz, 1H), 7.29 (t, *J* = 7.72 Hz, 1H), 7.09 (t, *J* = 7.32 Hz, 1H), 6.93 (d, *J* = 7.62 Hz, 1H), 5.08−5.20 (m, 1H), 3.81−3.94 (m, 2H), 3.64−3.79 (m, 3H), 3.51−3.61 (m, 2H), 2.72−2.80 (m, 2H), 1.93−2.06 (m, 2H), 1.67−1.83 (m, 2H). MS (ES+) *m/z*: 317.4.

1-(Methoxycarbonyl)piperidin-4-yl (3S,5′R)-2-Oxo-1,2-dihydrospiro[indole-3,3′-pyrrolidine]-5′-carboxylate (7). Prepared by method B from **19** (53 mg, 0.16 mmol) and methyl 4-hydroxy-piperidine-1-carboxylate (vide infra) (44 mg, 0.28 mmol) to afford **7** (11.8 mg, 18% over two steps) as an off-white solid. ¹H NMR (400 MHz, methanol-*d*₄) δ 7.47 (d, *J* = 6.64 Hz, 1H), 7.28 (t, *J* = 7.62 Hz, 1H), 7.09 (t, *J* = 7.03 Hz, 1H), 6.93 (d, *J* = 7.62 Hz, 1H), 5.09−5.25 (m, 1H), 4.92−5.07 (m, 1H), 3.56−3.82 (m, 7H), 3.34−3.52 (m, 2H), 2.62−2.90 (m, 2H), 1.82−1.99 (m, 2H), 1.58−1.82 (m, 2H). MS (ES+) *m/z*: 373.9.

Benzyl (3S,5′R)-2-Oxo-1,2-dihydrospiro[indole-3,3′-pyrrolidine]-5′-carboxylate (8). Prepared by method B from **19** (76 mg, 0.23 mmol) and benzyl alcohol (57 mg, 0.52 mmol) to afford **8** (11.9 mg, 12% over two steps) as a colorless glass. ¹H NMR (400 MHz, acetonitrile-*d*₃) δ 8.73 (br s, 1H), 7.34−7.46 (m, 6H), 7.30 (dt, *J* = 1.17, 7.72 Hz, 1H), 7.10 (dt, *J* = 0.98, 7.62 Hz, 1H), 6.96 (dd, *J* = 0.59, 7.81 Hz, 1H), 5.28 (s, 2H), 4.96 (dd, *J* = 4.49, 10.16 Hz, 1H), 3.74 (d, *J* = 12.11 Hz, 1H), 3.67 (d, *J* = 12.31 Hz, 1H), 2.78 (dd, *J* = 10.16, 14.06 Hz, 1H), 2.70 (dd, *J* = 4.20, 14.16 Hz, 1H). MS (ES+) *m/z*: 323.3.

4-Cyanobenzyl (3S,5′R)-2-Oxo-1,2-dihydrospiro[indole-3,3′-pyrrolidine]-5′- carboxylate (9). Prepared by method A from **19** (135 mg, 0.406 mmol) and 4-cyanobenzyl alcohol (97 mg, 0.73 mmol) to afford **9** (60 mg, 42% over two steps) after purification (Phenomenex HILIC (Diol) 250 mm × 21.2 mm 5 *μ*m column, 5−100% EtOH/heptanes over 8.5 min, 28 mL/min) as a colorless glass. ¹H NMR (500 MHz, methanol-*d*₄) δ 7.76 (d, *J* = 8.05 Hz, 2H), 7.64 (d, *J* = 8.30 Hz, 2H), 7.48 (d, *J* = 7.32 Hz, 1H), 7.31 (t, *J* = 7.81 Hz, 1H), 7.05−7.16 (m, 1H), 6.96 (d, *J* = 7.81 Hz, 1H), 5.45 (d, *J* = 13.18 Hz, 1H), 5.38 (d, *J* = 13.18 Hz, 1H), 5.02 (br s, 1H), 3.76 (d, *J* = 11.71 Hz, 1H), 3.66 (d, *J* = 12.45 Hz, 1H), 2.69−2.83 (m, 2H). MS (ES-API) *m/z*: 347.9.

4-Bromobenzyl (3S,5′R)-2-Oxo-1,2-dihydrospiro[indole-3,3′-pyrrolidine]-5′-carboxylate (10). Prepared by method A from **19** (36 mg, 0.10 mmol) and 4-bromobenzyl alcohol (25 mg, 0.13 mmol) to afford **10** (17 mg, 45% over two steps) after purification (Princeton Silica 250 mm × 21.2 mm 5 *μ*m column, 5−100% EtOH/heptane over 10 min, 28 mL/min) as a colorless glass. ¹H NMR (500 MHz, methanol-*d*₄) δ 7.52−7.56 (m, 2H), 7.34−7.39 (m, 3H), 7.25 (dt, *J* = 1.10, 7.75 Hz, 1H), 7.07 (dt, *J* = 0.98, 7.57 Hz, 1H), 6.93 (d, *J* = 7.81 Hz, 1H), 5.21−5.28 (m, 2H), 4.50 (dd, *J* = 7.20, 8.42 Hz, 1H), 3.52 (d, *J* = 11.71 Hz, 1H), 3.24 (d, *J* = 11.71 Hz, 1H), 2.50−2.60 (m, 2H). MS (ES+) *m/z*: 400.8 (M + H), 402.8 [(M + H) + 2].

3-Bromo-4-cyanobenzyl (3S,5′R)-2-Oxo-1,2-dihydrospiro[indole-3,3′-pyrrolidine]-5′-carboxylate (11). Prepared by method A from **19** (17 mg, 0.05 mmol) and 3-bromo-4-cyanobenzyl alcohol (12 mg, 0.055 mmol) to afford **11** (18.9 mg, 70% over two steps) as a white solid. ¹H NMR (400 MHz, acetonitrile-*d*₃) δ 8.71 (br s, 1H), 7.84 (dd, *J* = 0.39, 1.56 Hz, 1H), 7.78 (d, *J* = 8.01 Hz, 1H), 7.54 (tdd, *J* = 0.71, 1.49, 8.03 Hz, 1H), 7.42 (s, 1H), 7.31 (dt, *J* = 1.27, 7.76 Hz, 1H), 7.11 (dt, *J* = 0.98, 7.62 Hz, 1H), 6.97 (qd, *J* = 0.60, 7.81 Hz, 1H), 5.26−5.39 (m, 2H), 5.00 (dd, *J* = 4.59, 9.86 Hz, 1H), 3.72−3.80 (m, 1H), 3.66−3.71 (m, 1H), 2.78−2.86 (m, 1H), 2.72−2.78 (m, 1H). MS (ES+) *m/z*: 426.2 (M + H), 428.2 [(M + H) + 2].

(3S,5′R)-((R)-6-Bromothiochroman-4-yl) 2-Oxospiro[indoline-3,3′-pyrrolidine]-5′-carboxylate (12a) and (3S,5′R)-((S)-6-Bromo-thiochroman-4-yl) 2-Oxospiro[indoline-3,3′-pyrrolidine]-5′-carboxylate (12b). Prepared by method A from **19** (289 mg, 0.87 mmol) and (*R,S*)-6-bromo-thiochroman-4-ol⁵³ (250 mg, 1.02 mmol). After removal of the protecting group (see General Method) and purification (Princeton Silica 250 mm × 21.2 mm 5 *μ*m column, 5−100% EtOH/heptane over 10 min, 28 mL/min), compound **12** was obtained as a colorless glass (212 mg, 44% over two steps). The diastereomers were separated using

a Chiralcel OD-H column (250 mm × 20 mm, 55/45 CO₂/MeOH, 10 mL/min).

12a (retention time = 3.21 min) was recovered as a colorless gum (37.4 mg). ¹H NMR (400 MHz, methanol-*d*₄) δ 7.48 (d, *J* = 2.34 Hz, 1H), 7.25−7.32 (m, 2H), 7.17 (dt, *J* = 1.17, 7.71 Hz, 1H), 6.96−7.03 (m, 2H), 6.86 (d, *J* = 7.61 Hz, 1H), 6.02−6.05 (m, 1H), 4.22 (dd, *J* = 6.93, 8.49 Hz, 1H), 3.29−3.38 (m, 1H), 3.25 (d, *J* = 2.93 Hz, 1H), 3.01 (d, *J* = 11.51 Hz, 1H), 2.86−2.95 (m, 1H), 2.44−2.55 (m, 1H), 2.31−2.44 (m, 2H), 2.03−2.16 (m, 1H). MS (ES+) *m/z*: 459.0 (M + H), 461.0 [(M + H) + 2].

12b (retention time = 4.89 min) was recovered as a white solid (70.8 mg). ¹H NMR (400 MHz, methanol-*d*₄) δ 7.48−7.51 (m, 1H), 7.26−7.33 (m, 2H), 7.14−7.22 (m, 1H), 6.96−7.03 (m, 2H), 6.84−6.88 (m, 1H), 5.98−6.10 (m, 1H), 4.20 (dd, *J* = 6.83, 8.39 Hz, 1H), 3.31−3.38 (m, 1H), 3.16−3.24 (m, 1H), 2.98−3.03 (m, 1H), 2.86−2.92 (m, 1H), 2.37−2.52 (m, 3H), 2.01−2.10 (m, 1H). MS (ES+) *m/z*: 459.0 (M + H), 461.0 [(M + H) + 2].

(3S,5′R)-((R)-6-Bromo-1,1-dioxothiochroman-4-yl)-2-oxospiro-[indoline-3,3′-pyrrolidine]-5′-carboxylate (13a). Di-*tert*-butyldicar-boxylate (11.9 mg, 0.055 mmol) was added to a solution of **12a** (20.7 mg, 0.045 mmol) and TEA (6.50 *μ*L, 0.045 mmol) in THF (0.5 mL). After 3 h at room temperature, the reaction was diluted with water (1 mL) and extracted with ethyl acetate (3 × 1 mL). The combined organic phases were dried (Na₂SO₄), filtered, and concentrated to afford the *N*-Boc intermediate (25.2 mg, 100%). *m*CPBA (113 mg, 0.51 mmol) was added to a solution of the intermediate prepared above (37.1 mg, 0.066 mmol) in DCM (2.5 mL). After 16 h at room temperature, the solvent was removed. Column chromatography on silica (4 g) with 0−60% ethyl acetate/heptane afforded the desired sulfone intermediate (39.0 mg, 100%). Removal of the protecting group (see General Method) followed by purification (Sepax 3-ethyl pyridine 250 mm × 21.2 mm 5 *μ*m column, 5−100% EtOH/heptane over 10 min, 28 mL/min) afforded **13a** (8.8 mg) as a beige solid. ¹H NMR (400 MHz, methanol-*d*₄) δ 7.74−7.79 (m, 3H), 7.28−7.32 (m, 1H), 7.18 (td, *J* = 1.37, 7.71 Hz, 1H), 7.00 (td, *J* = 1.17, 7.61 Hz, 1H), 6.87 (d, *J* = 7.81 Hz, 1H), 6.18 (dd, *J* = 3.90, 5.27 Hz, 1H), 4.28 (t, *J* = 7.32 Hz, 1H), 3.67−3.78 (m, 1H), 3.57 (q, *J* = 7.02 Hz, 1H), 3.43−3.52 (m, 1H), 3.36 (d, *J* = 11.51 Hz, 1H), 3.04 (d, *J* = 11.51 Hz, 1H), 2.75−2.86 (m, 1H), 2.64−2.75 (m, 1H), 2.44 (s, 1H), 2.42 (s, 1H). LC/MS (ES+) *m/z*: 490.8 (M + H), 492.8 [(M + H) + 2].

(3S,5′R)-((S)-6-Bromo-1,1-dioxothiochroman-4-yl)-2-oxospiro-[indoline-3,3′-pyrrolidine]-5′-carboxylate (13b). Di-*tert*-butyldicar-boxylate (11.9 mg, 0.055 mmol) was added to a solution of **12b** (33.7 mg, 0.073 mmol) and TEA (10.5 *μ*L, 0.073 mmol) in THF (0.5 mL). After 3 h at room temperature, the reaction was diluted with water (1 mL) and extracted with ethyl acetate (3 × 1 mL). The combined organic phases were dried (Na₂SO₄), filtered, and concentrated to afford the *N*-Boc intermediate (39.7 mg, 97%). *m*CPBA (130 mg, 0.58 mmol) was added to a solution of the intermediate prepared above (39.7 mg, 0.071 mmol) in DCM (2.5 mL). After 16 h at room temperature, the solvent was removed. Column chromatography on silica (4 g) with 0−100% ethyl acetate/heptane afforded the desired sulfone intermediate (42 0.0 mg, 100%). Removal of the protecting group (see General Method) followed by purification (Sepax 3-ethyl pyridine 250 mm × 21.2 mm 5 *μ*m column, 5−100% EtOH/heptane over 10 min, 28 mL/min) afforded **13b** (11.3 mg) as a beige solid. ¹H NMR (400 MHz, DMSO-*d*₆) δ 10.41 (s, 1H), 7.71−7.87 (m, 3H), 7.33 (d, *J* = 7.42 Hz, 1H), 7.13 (dt, *J* = 1.17, 7.71 Hz, 1H), 6.87−6.95 (m, 1H), 6.79 (d, *J* = 7.61 Hz, 1H), 6.10 (dd, *J* = 4.10, 6.05 Hz, 1H), 4.30 (t, *J* = 7.42 Hz, 1H), 3.52−3.73 (m, 2H), 3.23−3.30 (m, 2H), 3.18 (d, *J* = 10.93 Hz, 1H), 2.93 (d, *J* = 10.93 Hz, 1H), 2.58−2.72 (m, 1H), 2.48−2.56 (m, 1H), 2.22−2.37 (m, 2H). LC/MS (ES+) *m/z*: 490.8 (M + H), 492.8 [(M + H) + 2].

1-Cyanocyclohexyl (3S,5′R)-2-Oxo-1,2-dihydrospiro[indole-3,3′-pyrrolidine]-5′-carboxylate (14). DCC (29 mg, 0.14 mmol) and DMAP (3.1 mg, 0.025 mmol) were added to a 0 °C suspension of **19** and 1-hydroxycyclohexanecarbonitrile (36 mg, 0.28 mmol) in DCM (3 mL). After stirring overnight at room temperature, the reaction was filtered through Celite and flash chromatographed (0−100% ethyl

acetate/heptane) to afford the Boc-intermediate (55 mg, 100%) as a white solid. MS (EI+) *m/z*: 440.4.

TFA (36 μL, 0.46 mmol) was added to a suspension of the Boc-intermediate in DCE (500 μL). After 18 h, the reaction was concentrated and purified by preparative RP HPLC (Waters Sunfire C18 ODB 5 μm 19 mm × 100 mm column; 15−80% MeCN/H$_2$O with 0.1% TFA) to afford **14** (7.4 mg, 35%) as a white foam. ^{1}H NMR (400 MHz, methanol-d_4) δ 7.39−7.49 (m, 1H), 7.32 (td, *J* = 1.27, 7.76 Hz, 1H), 7.11 (td, *J* = 1.17, 7.62 Hz, 1H), 6.96 (dt, *J* = 0.78, 7.81 Hz, 1H), 5.09 (dd, *J* = 5.27, 9.57 Hz, 1H), 3.78 (d, *J* = 12.11 Hz, 1H), 3.69 (d, *J* = 12.11 Hz, 1H), 2.78−2.85 (m, 1H), 2.70−2.78 (m, 1H), 2.25−2.44 (m, 2H), 1.96−2.09 (m, 2H), 1.73−1.88 (m, 2H), 1.52−1.72 (m, 3H), 1.41 (dd, *J* = 4.10, 10.55 Hz, 1H). MS (ES+) *m/z*: 339.9.

(3S,5′R)-5′-[(Benzyloxy)methyl]spiro[indole-3,3′-pyrrolidin]-2(1H)-one (15). Potassium *tert*-butoxide (1.0 M in THF, 1.4 mL, 1.4 mmol) was added dropwise under nitrogen to a 0 °C solution of **19** (512 mg, 1.45 mmol) in THF (10 mL). After 5 min, 2-(trimethylsilyl)-ethoxymethyl chloride (287 μL, 1.63 mmol) was added and the reaction was allowed to reach room temperature over 30 min. The reaction was diluted with ethyl acetate (10 mL) and saturated aqueous ammonium chloride (10 mL). The organic layer was removed, washed again with saturated aqueous ammonium chloride solution (10 mL), dried (MgSO$_4$), and concentrated at reduced pressure to a viscous oil. Purification by normal phase chromatography (40 g silica) with a 0−100% ethyl acetate/heptane gradient afforded **22** (501 mg, 71%) as a viscous oil.

Lithium borohydride solution (1.0 M in THF, 524 μL, 0.524 mmol) was added dropwise under nitrogen to a −20 °C solution of **22** (250 mg, 0.52 mmol) in THF (10 mL). The reaction was allowed to reach room temperature over 16 h. The reaction was then cooled to 0 °C (external temperature) and quenched carefully with 15% aqueous citric acid (20 mL) and ethyl acetate (20 mL). The layers were separated and the aqueous phase was extracted with ethyl acetate (2 × 5 mL). The combined organic phases were washed with aqueous 5% NaHCO$_3$ (2 × 25 mL), dried (MgSO$_4$), and concentrated to afford crude alcohol (311 mg) as a viscous oil. Purification by normal phase chromatography (40 g silica) using 1:3 ethyl acetate/heptane afforded **23** (64 mg, 27%) as a white foam.

Unwashed sodium hydride (60% dispersion in mineral oil, 6.0 mg, 0.15 mmol) was added at room temperature to a stirred solution of **23** (39 mg, 0.087 mmol) and benzyl bromide (75 mg, 0.44 mmol) in THF (1 mL). After 3 h, the reaction was diluted with ethyl acetate (5 mL) and saturated aqueous ammonium chloride (5 mL). The layers were separated, and the aqueous phase was extracted with ethyl acetate (2 × 5 mL). The combined organic phases were washed with aqueous 5% NaHCO$_3$ (5 mL) and brine (5 mL), dried (MgSO$_4$), and concentrated to afford the crude benzyl ether (48 mg) as a colorless oil. Purification by normal phase chromatography (4 g silica) using 1:3 ethyl acetate/heptane afforded **24** (25 mg, 53%) as a colorless oil.

Tetrabutylammonium fluoride (1.0 M in THF, 72 μL, 0.72 mmol) was added to a solution of **24** (13 mg, 0.024 mmol) in DMF (200 μL). After 1 h at 100 °C, the reaction was cooled, then cooled, then diluted with water (2 mL) and ethyl acetate (2 mL). The layers were separated, and the aqueous phase was extracted with ethyl acetate (2 × 1 mL). The combined organic phases were washed with 1N HCl (2 mL) and saturated aqueous NaHCO$_3$ (2 mL), dried MgSO$_4$, and concentrated to afford **25** (10 mg, quant.) as a clear colorless oil, which was used directly in the next step.

Boc-intermediate **25** (10 mg, 0.024 mmol) was dissolved in methanol (250 μL) and treated with 4 M HCl in dioxane (250 μL). After 1 h, the solvent was removed under reduced pressure and the residue purified by reverse phase chromatography to afford a clear film (4.4 mg). This was further purified by dissolving the material in methanol (1 mL) and applying to a 1000 mg SCX cartridge (JT Baker). The cartridge was washed with methanol (5 mL) and eluted with 1N ammonia in methanol (5 mL). The eluent was evaporated at reduced pressure, and the residue thus obtained was dissolved in methanol (250 μL) and treated with 4 M HCl in dioxane (250 μL). Removal of the solvent afforded **14** (3.5 mg, 42%) as the hydrochloride salt. ^{1}H NMR (400 MHz, methanol-d_4) δ 7.22−7.45 (m, 7H), 7.04−7.12 (m,

1H), 6.93 (d, *J* = 7.62 Hz, 1H), 4.58−4.70 (m, 2H), 4.34 (quin, *J* = 7.67 Hz, 1H), 3.80−3.86 (m, 2H), 3.68 (d, *J* = 12.89 Hz, 1H), 3.52 (d, *J* = 12.11 Hz, 1H), 2.38 (dd, *J* = 8.01, 13.48 Hz, 1H), 2.26 (dd, *J* = 9.67, 13.57 Hz, 1H). MS (ES+) *m/z*: 309.3.

(3S,5′S)-5′-(3-Phenylpropyl)spiro[indole-3,3′-pyrrolidin]-2(1H)-one (16). Lithium bis-(trimethylsilyl)amide solution (1.0 M in THF, 740 μL, 0.74 mmol) was added to a −78 °C suspension of phenethyltriphenylphosphonium bromide (340 mg, 0.76 mmol) in anhydrous THF (2 mL).[52] After 1 h at −78 °C, a solution of **21** (80 mg, 0.25 mmol) in anhydrous THF (2 mL) was added and the reaction allowed to reach room temperature overnight. After removal of solvent in vacuo, the residue was partitioned between ethyl acetate (15 mL) and water (20 mL). The aqueous was extracted with ethyl acetate (2 × 10 mL), and the combined organic phases were dried (Na$_2$SO$_4$) and concentrated to afford a yellow oil. Flash chromatography (0−100% ethyl acetate/heptanes) afforded the unsaturated intermediate (34 mg, 34%) as a colorless glass. MS (EI+) *m/z*: 404.9.

A 0.005 M solution of the alkene (12 mg, 0.03 mmol) in methanol was hydrogenated over 10% Pd/C using a Thales H-Cube (full hydrogen, 35 °C, 1.0 mL/min flow rate). Removal of the solvent afforded the saturated intermediate as a colorless glass (8.4 mg, 69%) which was carried on without further purification.

A solution of the Boc-intermediate prepared above (8.4 mg, 0.02 mmol) was dissolved in 4 M HCl/dioxane and stirred at room temperature for 4 h. The solvent was removed in vacuo and the residue dried under high vacuum to afford **16** as the hydrochloride salt in quantitative yield (7 mg). ^{1}H NMR (400 MHz, methanol-d_4) δ 7.39−7.46 (m, 1H), 7.21−7.33 (m, 5H), 7.15−7.21 (m, 1H), 7.07−7.14 (m, 1H), 6.95 (dd, *J* = 0.78, 7.81 Hz, 1H), 3.98−4.14 (m, 1H), 3.67−3.74 (m, 1H), 3.44−3.56 (m, 1H), 2.73 (t, *J* = 7.23 Hz, 2H), 2.45 (dd, *J* = 7.13, 13.57 Hz, 1H), 2.18 (dd, *J* = 10.35, 13.48 Hz, 1H), 1.86−2.02 (m, 1H), 1.74−1.86 (m, 2H), 1.16−1.50 (m, 1H). MS (ES+) *m/z*: 307.3.

(R)-Methyl 2,3,4,9-Tetrahydro-1H-pyrido[3,4-b]indole-3-carboxylate hydrochloride (17). To a stirring solution of D-tryptophan methyl ester hydrochloride (24.5 g, 96.1 mmol, 1.00 equiv) in methanol (250 mL) was added 37% aqueous formaldehyde solution (8.65 g, 55.0 mmol, 1.10 equiv) at room temperature. The resulting solution was stirred at reflux for 90 min. The total volume was reduced in vacuo to approximately 30 mL, whereupon a white precipitate formed. Methyl-*tert*-butyl ether (100 mL) was added, and the resulting white suspension was stirred for 15 min. The resulting solid was filtered then dried on high vacuum to afford the title compound **17** (22.3 g, 89% yield) as a fluffy white solid. ^{1}H NMR (400 MHz, DMSO-d_6) δ 11.18 (s, 1H), 10.17 (br s, 2H), 7.49 (d, *J* = 7.81 Hz, 1H), 7.38 (td, *J* = 0.93, 8.11 Hz, 1H), 7.12 (ddd, *J* = 1.17, 7.08, 8.15 Hz, 1H), 7.02 (ddd, *J* = 0.98, 7.03, 8.01 Hz, 1H), 4.64 (dd, *J* = 5.27, 10.16 Hz, 1H), 4.40 (s, 1H), 3.31 (dd, *J* = 5.27, 16.02 Hz, 1H), 3.07 (dd, *J* = 10.25, 15.92 Hz, 2H). MS (ES+) *m/z*: 231.3.

(3S,5′R)-1′-tert-Butyl 5′-Methyl 2-Oxospiro[indoline-3,3′-pyrrolidine]-1′,5′-dicarboxylate (18a). Triethylamine (23.0 mL, 165 mmol) was added rapidly to a stirring suspension of tetrahydro-*β*-carboline **17** (22.0 g, 82.0 mmol) in 2-methyltetrahydrofuran (200 mL) at 8 °C (internal temperature). Water (50 mL) was added, and the resulting clear and colorless turbid solution was stirred at 11 to 5 °C (internal temperature) for 20 min. Solid di-*tert*-butyl-dicarbonate (18.9 g, 84.1 mmol) was added in 10 portions (no exotherm was observed). The vessel containing the di-*tert*-butyl-dicarbonate was rinsed with 2-methyltetrahydrofuran (25 mL) and added to the reaction. The reaction mixture was stirred at 4−5 °C for 30 min, allowed to warm to room temperature, and stirred at room temperature for 90 min. Additional 2-methyltetrahydrofuran (225 mL) was added and then the reaction was cooled to 5 °C (internal temperature). Aqueous 1N HCl (85 mL) was slowly added, the phases were separated, and the upper organic layer was washed with saturated sodium bicarbonate solution (150 mL) followed by brine (100 mL). The organic layer was dried (MgSO$_4$) and filtered to afford the Boc-protected tetrahydro-*β*-carboline intermediate as a solution in 2-methyltetrahydrofuran (27.0 g, assumed quantitative, 0.182 M solution).

To the 0.182 M solution prepared above was added deionized water (200 mL) at 3 °C (internal temperature) followed by rapid addition of glacial acetic acid (67.0 mL, 1.17 mol). The stirring cloudy mixture was cooled to −1 °C (internal temperature), and solid N-bromosuccinimide (13.7 g, 76.2 mmol) was added in multiple potions, never allowing the internal temperature to exceed 2 °C during the additions. The reaction was stirred at 2 °C to −7 °C (internal temperature) over 30 min, during which time the slightly cloudy reaction mixture became a clear and colorless solution. The reaction was poured into a separation funnel containing saturated sodium bicarbonate solution (1.6 L). The contents were extracted and separated. The lower aqueous layer was washed with 2-methyltetrahydrofuran (300 mL), and then the combined upper organic extracts (~750 mL) were washed with brine (150 mL), dried over $MgSO_4$, filtered, and concentrated in vacuo to give a mixture of **18a** and **18b** (~12:1), which was subjected to careful normal-phase column chromatography to separate the diastereomers (**18b** elutes before **18a**) to afford **18a** (21.2 g, 75% yield from compound **17**) as a white solid. ^{1}H NMR (500 MHz, DMSO-d_6) δ 10.66 (s, 1H), 7.24 (t, J = 7.69 Hz, 1H), 7.08 (dd, J = 7.32, 19.28 Hz, 1H), 6.96−7.03 (m, 1H), 6.90 (d, J = 7.81 Hz, 1H), 4.56−4.66 (m, 1H), [3.73 (s) and 3.70 (s), 3H total, rotational isomers], 3.54−3.62 (m, 1H), 3.50 (t, J = 11.10 Hz, 1H), 2.50 (td, J = 1.83, 3.66 Hz, 1H), 2.39 (dd, J = 8.05, 12.69 Hz, 1H), 2.18−2.32 (m, 1H), [1.40 (s) and 1.38 (s), 9H total, rotational isomers]. 1D-NOESY (5′H ⟨−⟩ 4H and 4′H$_b$). MS (ES+) m/z: 347.0.

(3S,5′R)-1′-(tert-Butoxycarbonyl)-2-oxospiro[indoline-3,3′-pyrrolidine]-5′-carboxylic Acid (19). Lithium hydroxide (434 mg, 17.8 mmol) was added to a stirring solution of compound **18a** (4.10 g, 11.8 mmol) in tetrahydrofuran (32 mL) and water (5 mL) and stirred at room temperature for 24 h. Aqueous 1N HCl (20 mL) was added to the reaction, and the contents were extracted with ethyl acetate (2 × 25 mL). The combined upper organic extracts were washed with brine (20 mL), dried ($MgSO_4$), filtered, concentrated in vacuo, and dried on high vacuum to afford the title compound **19** (3.78 g, 96%) as a white solid. ^{1}H NMR (500 MHz, DMSO-d_6) δ 10.66 (s, 1H), 7.23 (dt, J = 1.22, 7.69 Hz, 1H), 6.97−7.09 (m, 2H, rotational isomers), 6.90 (d, J = 7.57 Hz, 1H), 4.44−4.54 (m, 1H), 3.44−3.62 (m, 2H, rotational isomers), 2.37 (ddd, J = 1.22, 8.05, 12.69 Hz, 1H), 2.17−2.30 (m, 1H), [1.41 (s) and 1.38 (s), 9H total, rotational isomers]. 1D-NOESY (5′H ⟨−⟩ 4H and 4′H$_b$; indicates no epimerization). MS (ES+) m/z: 333.2. MS (ES−) m/z: 331.1.

Methyl 4-Hydroxypiperidine-1-carboxylate. Potassium carbonate (5.64 g, 40.8 mmol) was added slowly to a 0 °C solution of 4-hydroxypiperidine (1.03 g, 10.2 mmol) in water (20 mL). Methyl chloroformate (3.15 mL, 40.9 mmol) was added dropwise. When the addition was complete, the cold bath was removed and the reaction was allowed to stir at room temperature for 1 h. The reaction was brought to pH 2 with 1 M HCl and extracted with DCE. The combined organic phases were dried ($MgSO_4$), filtered, and concentrated under reduced pressure to afford the product (0.932 g, 57%) as a colorless oil which was used without further purification. ^{1}H NMR (400 MHz, DMSO-d_6) δ 4.73 (d, J = 4.10 Hz, 1H), 3.58−3.74 (m, 3H), 3.56 (s, 3H), 2.94−3.09 (m, 2H), 1.61−1.73 (m, 2H), 1.18−1.33 (m, 2H). MS (APCI+) m/z: 160.1.

ASSOCIATED CONTENT

Accession Codes

Atomic coordinates and structure factors for the following BACE cocrystal structures have been deposited with the RCSB: compound **1** (3UDH), compound **5** (3UDJ), compound **6** (3UDK), compound **8** (3UDM), compound **9** (3UDN), compound **11** (3UDY), compound **12** (3UDP), compound **13a** (3UDQ), compound **14** (3UDR).

AUTHOR INFORMATION

Corresponding Author

*For I.V.E.: phone, +1 860 686 1373; fax, +1 860 686 7391; E-mail, ivan.efremov@pfizer.com. For F.F.V.: phone, +1 860 715 6504; E-mail, felix.vajdos@pfizer.com.

Present Addresses

†St. Joseph College, 1678 Asylum Avenue, West Hartford, Connecticut 06117, United States

‡Genentech, Inc., 1 DNA Way, South San Francisco, California 94080, United States

Notes

The authors declare no competing financial interest.

ABBREVIATIONS USED

AD, Alzheimer's Disease; ADME, absorption, distribution, metabolism, and excretion; APP, amyloid precursor protein; Aβ, amyloid β peptide; BACE, β-secretase, BACE1; CNS, central nervous system; FBDD, fragment-based drug discovery; HEA, hydroxyethyl amine; HLM, human liver microsomes; LE, ligand efficiency; MDCK, Madin−Darby canine kidney; MDR, multiple-drug resistant; MS, mass spectrum; MW, molecular weight; ND, not determined; NOE, nuclear Overhauser effect; P-gp, P-glycoprotein; RT, room temperature; SAR, structure−activity relationship; TSI, transition state isostere

REFERENCES

(1) Tiraboschi, P.; Hansen, L. A.; Thal, L. J.; Corey-Bloom, J. The importance of neuritic plaques and tangles to the development and evolution of AD. *Neurology* **2004**, 62 (11), 1984−1989.

(2) Hardy, J.; Allsop, D. Amyloid deposition as the central event in the aetiology of Alzheimer's disease. *Trends Pharmacol. Sci.* **1991**, 12, 383−388.

(3) Bredesen, D. E. Koo, E.H., BACE, APP Processing, and Signal Transduction in Alzheimer's Disease. In *BACE: Lead Target for Orchestrated Therapy of Alzheimer's Disease*; John, V., Ed.; John Wiley & Sons: Hoboken, NJ, 2010; pp 1−13.

(4) 2008 Alzheimer's disease facts and figures. *Alzheimer's Dementia* **2008**, 4(2), 110−133.

(5) Wolfe, M. S. The γ-Secretase Complex: Membrane-Embedded Proteolytic Ensemble. *Biochemistry* **2006**, 45 (26), 7931−7939.

(6) Eder, J.; Hommel, U.; Cumin, F.; Martoglio, B.; Gerhartz, B. Aspartic Proteases in Drug Discovery. *Curr. Pharm. Des.* **2007**, 13, 271−285.

(7) Tang, J.; James, M. N. G.; Hsu, I. N.; Jenkins, J. A.; Blundell, T. L. Structural evidence for gene duplication in the evolution of the acid proteases. *Nature* **1978**, 271 (5646), 618−621.

(8) Coates, L.; Erskine, P. T.; Mall, S.; Gill, R.; Wood, S. P.; Myles, D. A. A.; Cooper, J. B. X-ray, neutron and NMR studies of the catalytic mechanism of aspartic proteinases. *Eur. Biophys. J.* **2006**, 35, 559−566.

(9) Tomasselli, A. G.; Bienkowski, M. BACE Biological Assays. In *BACE: Lead Target for Orchestrated Therapy of Alzheimer's Disease*; John, V., Ed.; John Wiley and Sons: New York, 2009.

(10) Abramowitz, N.; Schechter, I.; Berger, A. On the size of the active site in proteases II. Carboxypeptidase-A. *Biochem. Biophys. Res. Commun.* **1967**, 29 (6), 862−867.

(11) Hong, L.; Koelsch, G.; Lin, X.; Wu, S.; Terzyan, S.; Ghosh, A. K.; Zhang, X. C.; Tang, J. Structure of the Protease Domain of

Memapsin 2 (β-Secretase) Complexed with Inhibitor. *Science* **2000**, *290* (5489), 150−153.

(12) Schechter, I.; Berger, A. On the size of the active site in proteinases. I. Papain. *Biochem. Biophys. Res. Commun.* **1967**, *27*, 157−162.

(13) Schechter, I.; Berger, A. On the active site of proteases. III. Mapping the active site of papain; specific peptide inhibitors of papain. *Biochem. Biophys. Res. Commun.* **1968**, *32* (5), 898−902.

(14) Turner, R. T.; Hong, L.; Koelsch, G.; Ghosh, A. K.; Tang, J. Structural Locations and Functional Roles of New Subsites S5, S6, and S7 in Memapsin 2 (β-Secretase). *Biochemistry* **2005**, *44* (1), 105−112.

(15) Congreve, M.; Aharony, D.; Albert, J.; Callaghan, O.; Campbell, J.; Carr, R. A. E.; Chessari, G.; Cowan, S.; Edwards, P. D.; Frederickson, M.; McMenamin, R.; Murray, C. W.; Patel, S.; Wallis, N. Application of Fragment Screening by X-ray Crystallography to the Discovery of Aminopyridines as Inhibitors of β-Secretase. *J. Med. Chem.* **2007**, *50* (6), 1124−1132.

(16) Edwards, P. D.; Albert, J. S.; Sylvester, M.; Aharony, D.; Andisik, D.; Callaghan, O.; Campbell, J. B.; Carr, R. A.; Chessari, G.; Congreve, M.; Frederickson, M.; Folmer, R. H. A.; Geschwindner, S.; Koether, G.; Kolmodin, K.; Krumrine, J.; Mauger, R. C.; Murray, C. W.; Olsson, L.-L.; Patel, S.; Spear, N.; Tian, G. Application of Fragment-Based Lead Generation to the Discovery of Novel, Cyclic Amidine β-Secretase Inhibitors with Nanomolar Potency, Cellular Activity, and High Ligand Efficiency. *J. Med. Chem.* **2007**, *50* (24), 5912−5925.

(17) Geschwindner, S.; Olsson, L.-L.; Albert, J. S.; Deinum, J.; Edwards, P. D.; de Beer, T.; Folmer, R. H. A. Discovery of a Novel Warhead against β-Secretase through Fragment-Based Lead Generation. *J. Med. Chem.* **2007**, *50* (24), 5903−5911.

(18) Kuglstatter, A.; Stahl, M.; Peters, J.-U.; Huber, W.; Stihle, M.; Schlatter, D.; Benz, J.; Ruf, A.; Roth, D.; Enderle, T.; Hennig, M. Tyramine fragment binding to BACE-1. *Bioorg. Med. Chem. Lett.* **2008**, *18* (4), 1304−1307.

(19) Murray, C. W.; Callaghan, O.; Chessari, G.; Cleasby, A.; Congreve, M.; Frederickson, M.; Hartshorn, M. J.; McMenamin, R.; Patel, S.; Wallis, N. Application of Fragment Screening by X-ray Crystallography to β-Secretase. *J. Med. Chem.* **2007**, *50* (6), 1116−1123.

(20) Chessari, G.; Woodhead, A. J. From fragment to clinical candidate—a historical perspective. *Drug Discovery Today* **2009**, *14* (13−14), 668−675.

(21) Hamada, Y.; Kiso, Y. Recent progress in the drug discovery of non-peptidic BACE1 inhibitors. *Expert Opin. Drug Discovery* **2009**, *4* (4), 391−416.

(22) Feng, B.; Mills, J. B.; Davidson, R. E.; Mireles, R. J.; Janiszewski, J. S.; Troutman, M. D.; de Morais, S. M. In Vitro P-glycoprotein Assays to Predict the in Vivo Interactions of P-glycoprotein with Drugs in the Central Nervous System. *Drug Metab. Dispos.* **2008**, *36* (2), 268−275.

(23) Coburn, C. A.; Stachel, S. J.; Li, Y.-M.; Rush, D. M.; Steele, T. G.; Chen-Dodson, E.; Holloway, M. K.; Xu, M.; Huang, Q.; Lai, M.-T.; DiMuzio, J.; Crouthamel, M.-C.; Shi, X.-P.; Sardana, V.; Chen, Z.; Munshi, S.; Kuo, L.; Makara, G. M.; Annis, D. A.; Tadikonda, P. K.; Nash, H. M.; Vacca, J. P.; Wang, T. Identification of a Small Molecule Nonpeptide Active Site β-Secretase Inhibitor That Displays a Nontraditional Binding Mode for Aspartyl Proteases. *J. Med. Chem.* **2004**, *47* (25), 6117−6119.

(24) Cole, D. C.; Manas, E. S.; Stock, J. R.; Condon, J. S.; Jennings, L. D.; Aulabaugh, A.; Chopra, R.; Cowling, R.; Ellingboe, J. W.; Fan, K. Y.; Harrison, B. L.; Hu, Y.; Jacobsen, S.; Jin, G.; Lin, L.; Lovering, F. E.; Malamas, M. S.; Stahl, M. L.; Strand, J.; Sukhdeo, M. N.; Svenson, K.; Turner, M. J.; Wagner, E.; Wu, J.; Zhou; Bard, J. Acylguanidines as Small-Molecule β-Secretase Inhibitors. *J. Med. Chem.,* **2006**, *49* (21), 6158−6161.

(25) Cole, D. C.; Stock, J. R.; Chopra, R.; Cowling, R.; Ellingboe, J. W.; Fan, K. Y.; Harrison, B. L.; Hu, Y.; Jacobsen, S.; Jennings, L. D.; Jin, G.; Lohse, P. A.; Malamas, M. S.; Manas, E. S.; Moore, W. J.; O'Donnell, M.-M.; Olland, A. M.; Robichaud, A. J.; Svenson, K.; Wu, J.; Wagner, E.; Bard, J. Acylguanidine inhibitors of β-secretase:

optimization of the pyrrole ring substituents extending into the S1 and S3 substrate binding pockets. *Bioorg. Med. Chem. Lett.* **2008**, *18* (3), 1063−1066.

(26) Fobare, W. F.; Solvibile, W. R.; Robichaud, A. J.; Malamas, M. S.; Manas, E.; Turner, J.; Hu, Y.; Wagner, E.; Chopra, R.; Cowling, R.; Jin, G.; Bard, J. Thiophene substituted acylguanidines as BACE1 inhibitors. *Bioorg. Med. Chem. Lett.* **2007**, *17* (19), 5353−5356.

(27) Baxter, E. W.; Conway, K. A.; Kennis, L.; Bischoff, F.; Mercken, M. H.; De Winter, H. L.; Reynolds, C. H.; Tounge, B. A.; Luo, C.; Scott, M. K.; Huang, Y.; Braeken, M.; Pieters, S. M. A.; Berthelot, D. J. C.; Masure, S.; Bruinzeel, W. D.; Jordan, A. D.; Parker, M. H.; Boyd, R. E.; Qu, J.; Alexander, R. S.; Brenneman, D. E.; Reitz, A. B. 2-Amino-3,4-dihydroquinazolines as Inhibitors of BACE-1 (β-Site APP Cleaving Enzyme): Use of Structure Based Design to Convert a Micromolar Hit into a Nanomolar Lead. *J. Med. Chem.* **2007**, *50* (18), 4261−4264.

(28) Pajouhesh, H.; Lenz, G. R. Medicinal Chemical Properties of Successful Central Nervous System Drugs. *NeuroRX* **2005**, *2* (4), 541−553.

(29) Wager, T. T.; Chandrasekaran, R. Y.; Hou, X.; Troutman, M. D.; Verhoest, P. R.; Villalobos, A.; Will, Y. Defining Desirable Central Nervous System Drug Space through the Alignment of Molecular Properties, in Vitro ADME, and Safety Attributes. *ACS Chem. Neurosci.* **2010**, *1* (6), 420−434.

(30) Lau, W. F.; Withka, J. M.; Hepworth, D.; Magee, T. V.; Du, J.; Bakken, G. A.; Miller, M. D.; Hendsch, Z. S.; Thanabal, V.; Kolodziej, S. A.; Xing, L.; Hu, Q.; Narasimhan, L. S.; Love, R.; Charlton, M. E.; Hughes, S.; Van Hoorn, W. P.; Mills, J. E. Design of a Multi-purpose Fragment Screening Library using Molecular Complexity and Orthogonal Diversity Metrics. *J. Comput.-Aided Mol. Des.* **2011**, 1−16.

(31) Tomasselli, A. G.; Paddock, D. J.; Emmons, T. L.; Mildner, A. M.; Leone, J. W.; Lull, J. M.; Cialdella, J. I.; Prince, D. B.; Fischer, H. D.; Heinrikson, R. L.; Benson, T. E. High Yield Expression of Human BACE Constructs in *Escherichia coli* for Refolding, Purification, and High Resolution Diffracting Crystal Forms. *Protein Pept. Lett.* **2008**, *15* (2), 131−143.

(32) Pflugrath, J. W. The finer things in X-ray diffraction data collection. *Acta Crystallogr., Sect. D: Biol. Crystallogr.* **1999**, *55*, 1718−1725.

(33) Bricogne, G.; Blanc, E.; Brandl, M.; Flensburg, C.; Keller, P.; Paciorek, W.; Roversi, P.; Smart, O. S.; Vonrhein, C.; , Womack, T. O., *BUSTER*; Global Phasing Ltd.: Cambridge, UK, 2009.

(34) Barrow, J. C.; Stauffer, S. R.; Rittle, K. E.; Ngo, P. L.; Yang, Z.; Selnick, H. G.; Graham, S. L.; Munshi, S.; McGaughey, G. B.; Holloway, M. K.; Simon, A. J.; Price, E. A.; Sankaranarayanan, S.; Colussi, D.; Tugusheva, K.; Lai, M.-T.; Espeseth, A. S.; Xu, M.; Huang, Q.; Wolfe, A.; Pietrak, B.; Zuck, P.; Levorse, D. A.; Hazuda, D.; Vacca, J. P. Discovery and X-ray Crystallographic Analysis of a Spiropiperidine Iminohydantoin Inhibitor of β-Secretase. *J. Med. Chem.* **2008**, *51* (20), 6259−6262.

(35) Freskos, J. N.; Fobian, Y. M.; Benson, T. E.; Bienkowski, M. J.; Brown, D. L.; Emmons, T. L.; Heintz, R.; Laborde, A.; McDonald, J. J.; Mischke, B. V.; Molyneaux, J. M.; Moon, J. B.; Mullins, P. B.; Bryan Prince, D.; Paddock, D. J.; Tomasselli, A. G.; Winterrowd, G. Design of potent inhibitors of human β-secretase. Part 1. *Bioorg. Med. Chem. Lett.* **2007**, *17* (1), 73−77.

(36) Maillard, M. C.; Hom, R. K.; Benson, T. E.; Moon, J. B.; Mamo, S.; Bienkowski, M.; Tomasselli, A. G.; Woods, D. D.; Prince, D. B.; Paddock, D. J.; Emmons, T. L.; Tucker, J. A.; Dappen, M. S.; Brogley, L.; Thorsett, E. D.; Jewett, N.; Sinha, S.; John, V. Design, Synthesis, and Crystal Structure of Hydroxyethyl Secondary Amine-Based Peptidomimetic Inhibitors of Human β-Secretase. *J. Med. Chem.* **2007**, *50* (4), 776−781.

(37) Hopkins, A. L.; Groom, C. R.; Alex, A. Ligand efficiency: a useful metric for lead selection. *Drug Discovery Today* **2004**, *9* (10), 430−431.

(38) Wang, Y.-S.; Liu, D.; Wyss, D. F. Competition STD NMR for the detection of high-affinity ligands and NMR-based screening. *Magn. Reson. Chem.* **2004**, *42* (6), 485−489.

(39) Liu, D.; Wang, Y.-S.; Gesell, J. J.; Wilson, E.; Beyer, B. M.; Wyss, D. F. Letter to the Editor: Backbone Resonance Assignments of the 45.3 kDa Catalytic Domain of Human BACE1. *J. Biomol. NMR* **2004**, *29* (3), 425−426.

(40) O'Neill, B. T. B., James, G.; Brodney, M. A.; Chenard, L. K.; Coffman, K. J.; Deng, B.; Dorff, P. H.; Efremov, I.; Kauffman, G. W.; Kleinman, E. F.; Lanyon, L. F.; Lin, W.; Liston, D.; Mansour, M.; Martin, B. A.; Martinez Alsina, L.; McColl, A. S.; Murray, J. C.; Oborski, C. E.; Sahagan, B. G.; Vajdos, F.; Wessel, M. D Pyrrolidine *β*-secretase inhibitors for treatment of Alzheimer's disease. 239th ACS National Meeting, San Francisco, CA, March 21−25, 2010.

(41) Congreve, M.; Aharony, D.; Albert, J.; Callaghan, O.; Campbell, J.; Carr, R. A. E.; Chessari, G.; Cowan, S.; Edwards, P. D.; Frederickson, M.; McMenamin, R.; Murray, C. W.; Patel, S.; Wallis, N. Application of Fragment Screening by X-ray Crystallography to the Discovery of Aminopyridines as Inhibitors of *β* -Secretase. *J. Med. Chem.* **2007**, *50* (6), 1124−1132.

(42) Sealy, J. M.; Truong, A. P.; Tso, L.; Probst, G. D.; Aquino, J.; Hom, R. K.; Jagodzinska, B. M.; Dressen, D.; Wone, D. W. G.; Brogley, L.; John, V.; Tung, J. S.; Pleiss, M. A.; Tucker, J. A.; Konradi, A. W.; Dappen, M. S.; Toth, G.; Pan, H.; Ruslim, L.; Miller, J.; Bova, M. P.; Sinha, S.; Quinn, K. P.; Sauer, J.-M. Design and synthesis of cell potent BACE-1 inhibitors: structure−activity relationship of P1′ substituents. *Bioorg. Med. Chem. Lett.* **2009**, *19* (22), 6386−6391.

(43) Truong, A. P.; Probst, G. D.; Aquino, J.; Fang, L.; Brogley, L.; Sealy, J. M.; Hom, R. K.; Tucker, J. A.; John, V.; Tung, J. S.; Pleiss, M. A.; Konradi, A. W.; Sham, H. L.; Dappen, M. S.; Tóth, G.; Yao, N.; Brecht, E.; Pan, H.; Artis, D. R.; Ruslim, L.; Bova, M. P.; Sinha, S.; Yednock, T. A.; Zmolek, W.; Quinn, K. P.; Sauer, J.-M. Improving the permeability of the hydroxyethylamine BACE-1 inhibitors: structure−activity relationship of P2′ substituents. *Bioorg. Med. Chem. Lett.* **2010**, *20* (16), 4789−4794.

(44) Wang, Y.-S.; Strickland, C.; Voigt, J. H.; Kennedy, M. E.; Beyer, B. M.; Senior, M. M.; Smith, E. M.; Nechuta, T. L.; Madison, V. S.; Czarniecki, M.; McKittrick, B. A.; Stamford, A. W.; Parker, E. M.; Hunter, J. C.; Greenlee, W. J.; Wyss, D. F. Application of Fragment-Based NMR Screening, X-ray Crystallography, Structure-Based Design, and Focused Chemical Library Design to Identify Novel *μ*M Leads for the Development of nM BACE-1 (*β*-Site APP Cleaving Enzyme 1) Inhibitors. *J. Med. Chem.* **2009**, *53* (3), 942−950.

(45) Kuglstatter, A.; Hennig, M. Fragment-Based Approaches for Identification of BACE Inhibitors. In *BACE: Lead Target for Orchestrated Therapy of Alzheimer's Disease*; John, V., Ed.; John Wiley & Sons, Inc: Hoboken, NJ, 2010; pp107−121.

(46) Blum, A.; Böttcher, J.; Heine, A.; Klebe, G.; Diederich, W. E. Structure-Guided Design of C2-Symmetric HIV-1 Protease Inhibitors Based on a Pyrrolidine Scaffold. *J. Med. Chem.* **2008**, *51* (7), 2078−2087.

(47) Böttcher, J.; Blum, A.; Dörr, S.; Heine, A.; Diederich, W.; Klebe, G. Targeting the Open-Flap Conformation of HIV-1 Protease with Pyrrolidine-Based Inhibitors. *ChemMedChem* **2008**, *3* (9), 1337−1344.

(48) Specker, E.; Böttcher, J.; Brass, S.; Heine, A.; Lilie, H.; Schoop, A.; Müller, G.; Griebenow, N.; Klebe, G. Unexpected Novel Binding Mode of Pyrrolidine-Based Aspartyl Protease Inhibitors: Design, Synthesis and Crystal Structure in Complex with HIV Protease. *ChemMedChem* **2006**, *1* (1), 106−117.

(49) Specker, E.; Böttcher, J.; Lilie, H.; Heine, A.; Schoop, A.; Müller, G.; Griebenow, N.; Klebe, G. An Old Target Revisited: Two New Privileged Skeletons and an Unexpected Binding Mode For HIV-Protease Inhibitors. *Angew. Chem., Int. Ed.* **2005**, *44* (20), 3140−3144.

(50) Stachel, S. J.; Steele, T. G.; Petrocchi, A.; Haugabook, S. J.; McGaughey, G.; Katharine, M.; Holloway, T.; Allison, S.; Munshi, P.; Zuck, D.; Colussi, K.; Tugasheva, A.; Wolfe, S. L.; Graham; Vacca, J. P. Discovery of pyrrolidine-based *β*-secretase inhibitors: Lead advancement through conformational design for maintenance of ligand binding efficiency. *Bioorg. Med. Chem. Lett.* **2012**, *22* (1), 240−244.

(51) Emsley, P.; Cowtan, K. Coot: Model-Building Tools for Molecular Graphics. *Acta Crystallogr., Sect. D: Biol. Crystallogr.* **2004**, *60*, 2126−2132.

(52) Lambert, J. B.; Mark, H. W.; Magyar, E. S. Inductive enhancement of aryl participation. *J. Am. Chem. Soc.* **1977**, *99* (9), 3059−3067.

(53) Grüninger-Leitch, F.; Schlatter, D.; Küng, E.; Nelböck, P.; Döbeli, H. Substrate and Inhibitor Profile of BACE (*β*-Secretase) and Comparison with Other Mammalian Aspartic Proteases. *J. Biol. Chem.* **2002**, *277*, 4687−4693.

(54) May, P. C.; Dean, R. A.; Lowe, S. L.; Martenyi, F.; Sheehan, S. M.; Boggs, L. N.; Monk, S. A.; Mathes, B. M.; Mergott, D. J.; Watson, B. M.; Stout, S. L.; Timm, D. E.; LaBell, E. S.; Gonzales, C. R.; Nakano, M.; Jhee, S. S.; Yen, M.; Ereshefsky, L.; Lindstrom, T. D.; Calligaro, D. O.; Cocke, P. J.; Hall, D. G.; Friedrich, S.; Citron, M.; Audia, J. E. Robust Central Reduction of Amyloid-*β* in Humans with an Orally Available, Non-Peptidic *β*-Secretase Inhibitor. *J. Neurosci.* **2011**, *31* (46), 16507−16516.